UPO

UNIVERSITÀ DEL PIEMONTE ORIENTALE

SCHOOL OF MEDICINE

Department of Health Science

Master Degree in Medical Biotechnologies

Master Thesis

***The role of IFI16 in modulating the immune response
upon HCoV infection***

Mentor: **Prof.ssa Cinzia BORGOGNA**

Firmato digitalmente da Cinzia Borgogna
Data: 27.02.2024 10:56:14 CET
Organizzazione: UNIVERSITA' DEGLI
STUDI DEL PIEMONTE
ORIENTALE/01943490027

Candidate: **Noor-E-Jannat Shorna**
Matricula: 20048061

Academic Year 2022/2023

Index

SUMMARY

Bats are the only mammals capable of sustained flight and are notorious reservoir hosts for some world's most highly pathogenic viruses, including coronaviruses (CoV). Genetic changes during the evolution of bats have included adaptations to limit collateral damage caused by by-products of elevated metabolic rate during flight. Notably, the entire locus encoding the Pyrin and HIN domain (PYHIN) family of proteins has been lost in bats. Interestingly, the host nuclear factor Interferon-γ-Inducible protein 16 (IFI16) has been reported to function as an antiviral restriction factor against several DNA viruses, such as human papillomavirus, human cytomegalovirus, and herpes simplex virus type 1, and in sensing of both DNA and RNA viruses. As these key innate defense pathways are deleted or nonfunctional in bats, our hypothesis is that their lack or impairment may contribute to the peaceful coexistence of CoV in bats without being detrimental for the host.

In this context, our aim was to investigate the role of IFI16 in modulating the host innate immune response upon human CoV (HCoV), using the bat-derived, low pathogenic NL63. These experiments were carried out in transfected control (TC) and IFI16 knock-out (KO) LLC-MK2 cells. In addition, a part of this thesis focused on the characterization of NL63 infection in a gold-standard cell line, namely LLC-MK2, due to the scarcity of information concerning the virus.

Our results demonstrated that in absence of IFI16, NL63 replicates less and reduces the transcription of viral genes, in accordance with reduced expression levels of the viral nucleoprotein. Also, in LLC-MK2 IFI16 KO cells we found an increase in the expression of innate immunity genes, upon NL63 infection. Moreover, in NL63-infected LLC-MK2 cells, we observed the translocation of IFI16 to the cytoplasm, where it colocalized with NP and by immunoprecipitation assay we confirmed the interaction of IFI16 with NP.

Overall, the results obtained indicate that the IFI16 protein may interfere with HCoV sensing with ensuing impact on the innate immune response during HCoV infection. The long-range goal of this project is to deepen our understanding of the role of IFI16 in triggering abnormal inflammatory reactions in HCoV-infected human epithelial cells. This understanding will help develop novel therapeutic approaches not only for HCoV-related diseases but also for other RNA virus diseases.

1.INTRODUCTION

1.1 Coronaviruses

1.1.1 General features and classification of coronaviruses

Coronaviruses are a family of enveloped, positive-sense, single-stranded RNA (+ssRNA) viruses known to infect birds and mammals, including bats and humans (Hartenian *et al*., 2020). Coronaviruses represent the largest virus group within the order of *Nidovirales*, in the family *Coronaviridae* and subfamily *Arteriviridae* (Masters and Perlman, 2013).

Based on their phylogenetic relationship and genomic structure, coronaviruses are categorized into four genera: Alphacoronavirus, Betacoronavirus, Gammacoronavirus, and Deltacoronavirus (Figure 1). Of these four genera, Alpha and Betacoronaviruses exclusively infect mammalian species (Cui *et al*., 2019; Xin *et al*., 2019). The Betacoronavirus genus is further classified into five lineages: *Embecovirus*, *Sarbecovirus*, *Merbecovirus*, *Nobecovirus*, and *Hibecovirus*.
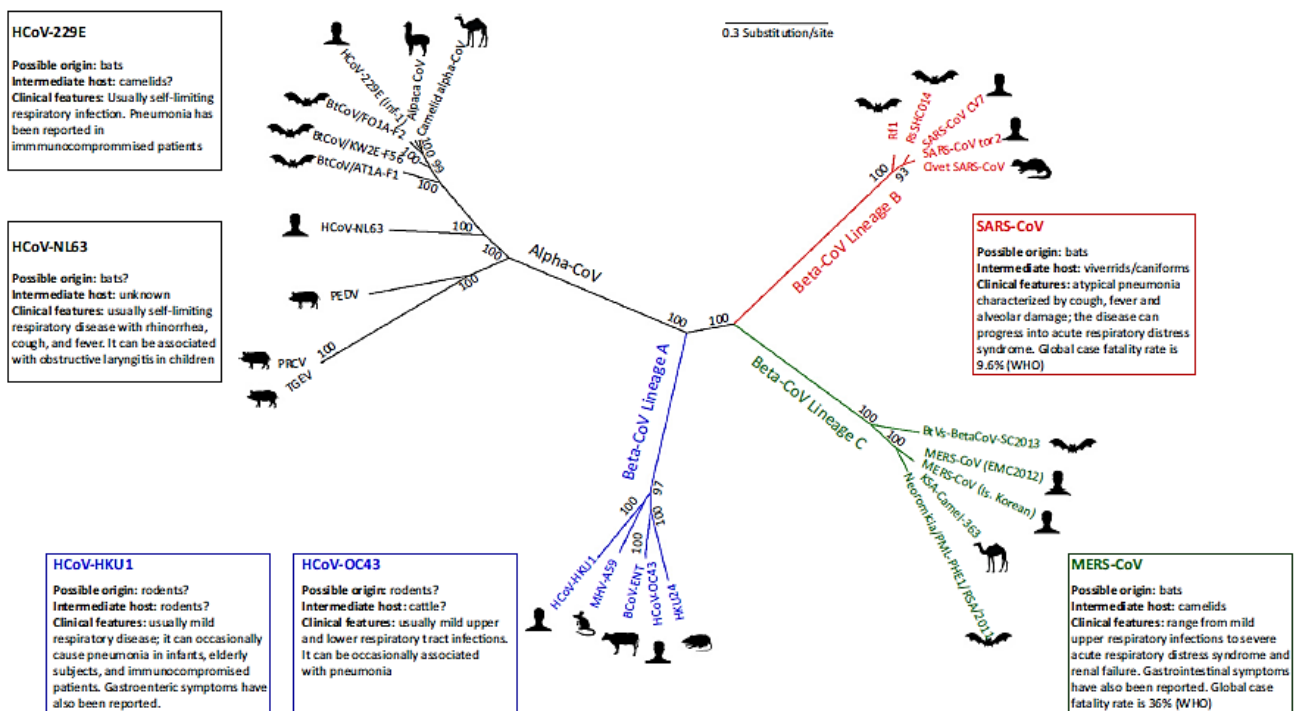
Figure 1. **Phylogenetic relationship and genome organization of human and animal coronaviruses**. The phylogenetic tree of complete genome sequences of HCoVs and selected mammalian CoVs was obtained with RAxML 8.2.4. Numbers indicate bootstrap support. CoVs are colored according to genus and lineage. Information about origin, intermediate host, and clinical presentation is reported for the six HCoVs. Data about case fatality rate were derived from the World Health Organization website (adapted from Forni *et al*., 2017).

Until now, only seven coronaviruses have been proven to be able to infect humans: HCoV-229E, HCoV-NL63, HCoV-OC43, HCoV-HKU1, SARS-CoV, MERS-CoV, and SARS-CoV-2. Depending on their infectivity, HCoVs are classified as high or low pathogenic. 229E, NL63, OC43, and HKU1 are considered low pathogenic HCoVs as they infect the upper respiratory tract causing mild to moderate respiratory infections in healthy individuals. On the other hand, highly pathogenic SARS-CoV, MERS-CoV, and SARS-CoV-2 infect the lower respiratory tract, and may be responsible of fatal illnesses, such as acute lung injury (ALI), acute respiratory distress syndrome (ARDS) or severe pneumonia (Chen *et al.*, 2020).

HCoV-229E and HCoV-OC43 were the first HCoVs to be isolated, in 1962 and 1965 respectively (Hamre and Procknow, 1966; McIntosh *et al.*, 1967). Before 2002, these were the only two coronaviruses known to be circulating in human population and they were considered relatively harmless since they caused mild illnesses. In 2002, a new HCoV emerged in South China and was responsible for severe respiratory infections with a fatality rate of 11% (hence, the name severe acute respiratory syndrome [SARS]-CoV) (Mulabbi *et al.*, 2021). In 2003, other two strains of HCoVs (NL63 and HUK1) were isolated from individuals with infections of the upper respiratory tract (Hoek *et al.*, 2004; Woo *et al.*, 2005). In 2012, a new highly pathogenic coronavirus, named Middle East Respiratory Syndrome (MERS)-CoV, appeared in Saudi Arabia, causing a series of severe lower respiratory tract infections, with a fatality rate of 35%. Unlike SARS-CoV, that disappeared a year after its emergence, MERS-CoV has remained causing outbreaks in the Middle East and in South Korea (Berry *et al.*, 2015; Fehr and Perlman, 2015). In the late 2019, a novel HCoV resembling SARS-CoV was discovered in the Hubei Province in China and was named SARS-CoV-2 (Zhu *et al.*, 2020). This new virus, responsible for the coronavirus disease 19 (COVID 19), rapidly spread worldwide, being declared a pandemic by the World Health Organization (WHO) in March 2020 (Adil *et al.*, 2021).

All coronaviruses circulating in humans have animal origins (Figure 2): SARS-CoV, MERS-CoV, SARS-CoV2, HCoV-NL63 and HCoV-229E originate in bats, whereas HCoV-OC43 and HCoV-HKU1 originate from rodents (Cui *et al.*, 2019; Artika *et al.*, 2020). Recent advancements in coronavirus research identified that bats harbor more than 200 novel coronaviruses, able to infect both humans and animals (Banerjee *et al.*, 2019).

HCoVs are transmitted through an animal-to-human spillover event, using intermediate hosts: civets for SARS-CoV, dromedary camels for MERS-CoV, Malayan pangolins for SARS-CoV-2, alpaca for HCoV-229E, and bovines for HCoV-OC43 (Cui *et al.*, 2019; Islam *et al.*, 2021). Until now, no concrete evidence exists on the intermediate host(s) of HCoV-NL63 and HCoV-
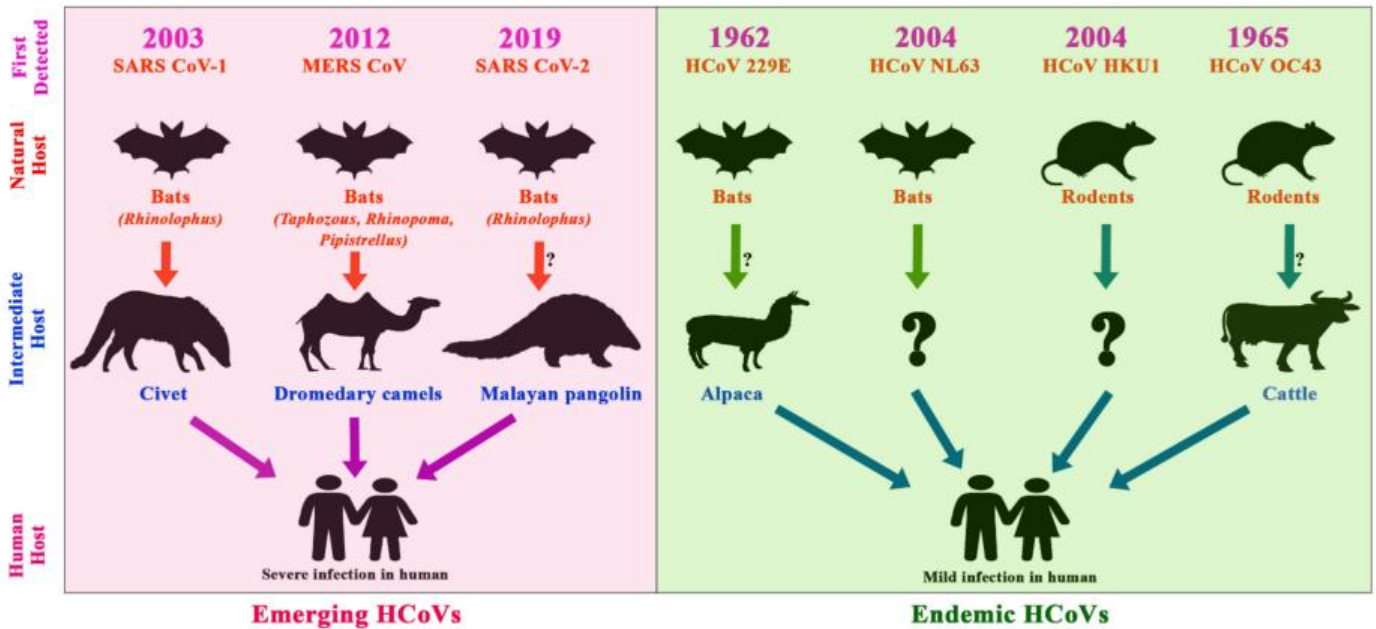

HKU1 (Ye *et al.*, 2020).

Figure 2. <u>Timeline of the emergence of HCoVs, their natural reservoirs, and intermediate hosts</u>. In the left are reported the emerging HCoVs (SARS-CoV, MERS-CoV and SARS-CoV-2) causing severe infection in humans, while in the right are depicted the endemic ones (HCoV-229E, HCoV-NL63, HCoV-HKU1 and HCoV-OC43) responsible of mild infection in humans. For each HCoV is reported the year of their first detection, the natural host, and the arrows represent the transmission of HCoVs from their natural hosts to the intermediate hosts, and eventually to the human population.

(adapted from Islam *et al.*, 2021).

Given all the spillover events occurred until now and the wide distribution of coronaviruses among various animal populations, it is likely that coronaviruses will continue to be a public health threat (Ruiz-Aravena *et al.*, 2021). Additionally, increased human-animal contact or interaction resulting from changes in human and animal behavior, habitat, pathogen adaptability, change in farm practices, urbanization, deforestation, and climate change, will increase the risk for the emergence of new zoonotic diseases, including those mediated by coronaviruses (Rahman *et al.*, 2020).

1.1.2 Coronavirus structure and genome organization

Coronavirus particles have a spherical morphology with a diameter of approximately 80-120 nm and comprise four major structural proteins: the nucleocapsid (N), the spike (S), the membrane (M), and the envelope (E) (Figure 3). These proteins have important functions in different steps of viral replication cycle, as well as maintaining the virus structure. While the viral envelope is made up of a lipid bilayer in which M, E and S are anchored, inside the virion, the helical nucleocapsid consists of multiple copies of the N protein associated with the
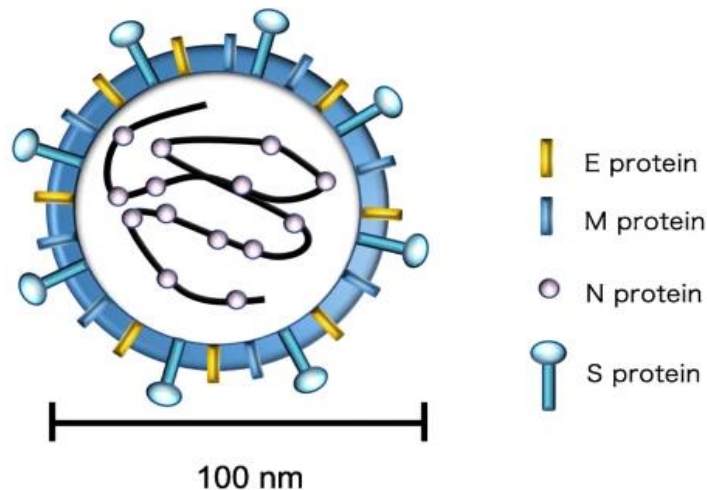
RNA genome (Deng and Baker, 2021)

Figure 3. <u>Schematic diagram of coronavirus virion</u>. The four major structural proteins of coronavirus particles are: S, spike glycoprotein; M, membrane glycoprotein; E, envelope protein; N, nucleocapsid phosphoprotein which encapsulates the single-stranded RNA genome (adapted from Kase and Okano, 2021).

Coronavirus genomes are known to be the biggest among RNA viruses, with a size ranging from 26 to 32 kb according to the genus. The genome consists of a single-stranded RNA molecule with positive polarity that resembles eukaryotic messenger RNAs (mRNAs) as it possesses a 5' cap and a 3' poly-A tail (Masters, 2006).

All coronaviruses' genomes share the same gene order: 5'-replicase-S-E-M-N-3' (Figure 4), encompassing multiple open reading frames (ORFs) that encodes a fixed array of structural and nonstructural proteins (NSPs), as well as various accessory proteins, which differ among the virus genera. The 5' end of the genome is occupied by two overlapping ORFs: ORF1a and ORF1b, carrying the information to synthesize two polypeptides (pp1a and pp1ab), which are subsequently cleaved to produce 16 NSPs; the remaining part of the genome at the 3' end is transcribed into subgenomic RNAs (sgRNAs) containing ORFs for the structural proteins: S, E,

M, N. Besides that, the 3 'end contains additional ORFs designated to encode a variable number of accessory proteins (Forni *et al*., 2017).

The accessory proteins of coronaviruses consist in a highly variable set of virus-specific proteins, that are principally thought to contribute to modulating host responses to infection and are determinants of viral pathogenicity. Nevertheless, the molecular functions of many accessory proteins remain largely unknown (Artika *et al*., 2020).
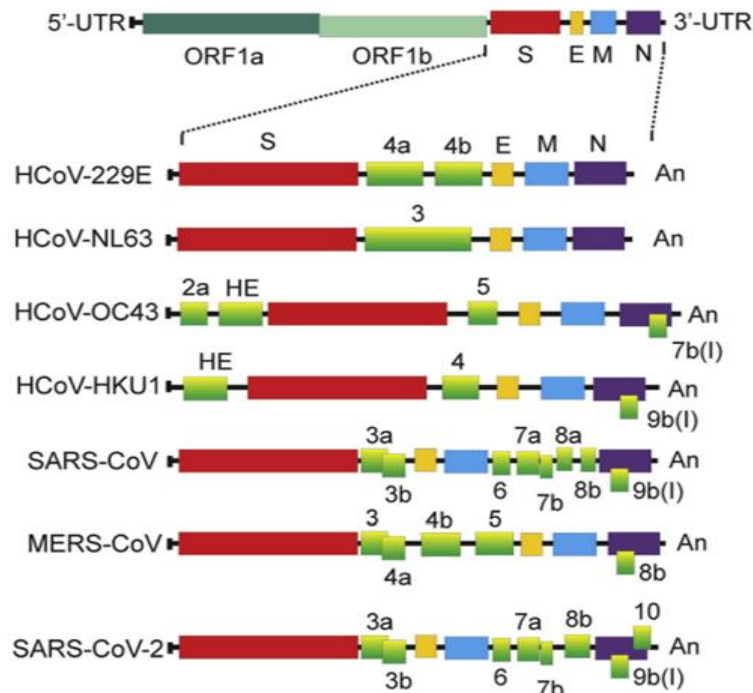

Figure 4. <u>Schematic structure of the complete genome of the seven HCoVs</u>. The replicase gene at the 5' end comprises two open reading frames: ORF-1a and ORF-1b. Whereas the 3' end contains ORFs for the structural proteins S, E, M, and N, in addition to ORFs for different accessory proteins. The extended regions downstream show the genome of two Alphacoronaviruses (299E and NL63) and five Betacoronaviruses (OC43, SARS-CoV, MERS-CoV, and SARS-CoV-2 (adapted from Artika *et al*., 2020)

1.1.3 Coronavirus lifecycle

The initial step of coronavirus infection involves the specific binding of the coronavirus S protein to the cellular viral entry receptors (Hoffmann *et al*., 2020), which have been identified for several coronaviruses, and include: aminopeptidase N (APN, CD13) for HCoV-229E, angiotensin-converting enzyme 2 (ACE2) used by HCoV-NL63, SARS-CoV and SARS-CoV-2, and dipeptidyl peptidase 4 (DPP4) for MERS-CoV (Millet *et al*., 2021). The expression and tissue distribution of entry receptors consequently influence the viral tropism and pathogenicity (Najafi *et al*., 2021).

Upon interaction with cellular receptor, the entry of the virus inside the cell is achieved through the fusion of the viral and cellular membranes, a process that starts as soon as the S protein is cleaved by host's proteases. After the viral attachment and membrane fusion, the viral nucleocapsid is released to the host cell cytoplasm through an uncoating process, and initiates the replication cycle (Chen *et al*., 2020). As the RNA genome of coronavirus reaches the cytoplasm, ORF1a and ORF1b are directly translated by cellular ribosomes into two big polyproteins: pp1a and pp1ab.

These polypeptides are further processed by viral proteases into 16 NSPs, which assemble to form the coronavirus replicase-transcriptase complex (RTC), that amplifies gRNA and sgRNAs. One important NSP is the RNA-dependent RNA polymerase (RdRp), which ensures replication of the full-length RNA, as well as the synthesis of sgRNA, encoding for structural and accessory proteins (Hartenian *et al*., 2020; V'kovski *et al*., 2021).

Replication of coronavirus genome requires the synthesis of complementary full-length negative-strand RNA, which serves as template for generation of positive-strand progeny genomes (Artika *et al*., 2020). In contrast, sgRNAs are formed by a process known as discontinuous transcription, by which each sgRNA is formed by a 5' leader sequence corresponding to the 5' end of the genome, joined to a mRNA body corresponding to sequences from the 3'-poly(A) stretch to a position that is upstream of each genomic ORF (Sawicki *et al*., 2007).

A distinctive feature of coronaviruses is that, unlike most enveloped viruses that assemble at the host cell plasma membrane, their assembly and budding occur at the endoplasmic reticulum-Golgi intermediate compartment (ERGIC), from which they acquire the viral envelope (Artika *et al*., 2020). Indeed, following their translation, the four viral structural proteins enter the secretory pathway in the ERGIC and insert into its membrane (Woo *et al*., 2019). The ERGIC is also the location where the viral genomes are encapsidated by the N protein. Thus, interaction of encapsidated viral genomes with structural proteins results in the assembly and budding of mature coronavirus particles from the ERGIC; finally, newly formed virions are secreted from the infected cell by exocytosis (Figure 5) (Fehr and Perlman, 2015).
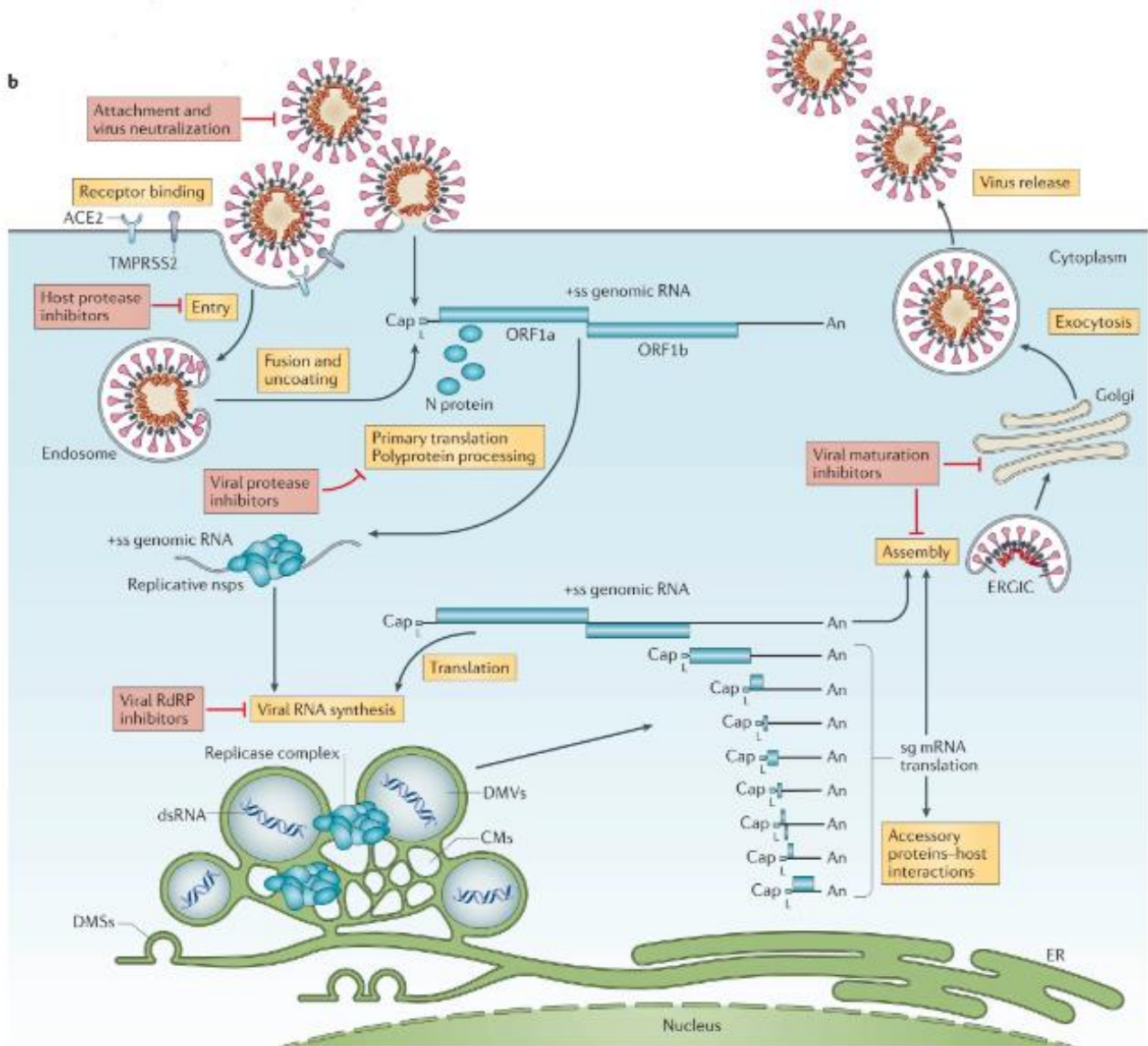
Figure 5. <u>**Schematic representation of coronavirus lifecycle**</u>. The step that initiates coronavirus infection is the binding of S proteins to the cellular receptors, that allows the fusion of the viral and host membranes. Subsequently the viral RNA is uncoated and enters in the cellular cytoplasm, ORF1a and ORF1b are translated to produce pp1a and pp1ab, which are then processed to produce 16 NSPs, that will form the RTC. The RTC drives the generation of negative-sense RNA through transcription and replication. During transcription, sgRNAs are produced, including those encoding all structural proteins. Structural proteins assemble into the nucleocapsid and viral envelope at the ERGIC, and finally newly produced virus particles are released from the infected cells by exocytosis (adapted from V'kovski *et al.*, 2021).

1.1.4 Human coronavirus NL63

Human coronavirus NL63 (HCoV-NL63) is an Alphacoronavirus that was first identified in 2003 in a 7-month-old child manifesting bronchiolitis and conjunctivitis (Hoek *et al.*, 2004). Since then, many other cases of HCoV-NL63 infection have been reported, indicating its

presence worldwide. Although it has been proven that HCoV-NL63 originated from bats, the intermediate host has not been identified yet (Ye *et al.*, 2020).

HCoV-NL63, along with other two coronaviruses (HCoV-229E and HCoV-OC43), is responsible for 10-30% of common cold cases, every year during winter season. In the vast majority of the cases, HCoV-NL63 infection only involves the upper respiratory tract, causing mild symptoms like fever, cough, sore throat, and rhinitis. Nonetheless, it can cause a more severe clinical picture in young children, elderly, and immunocompromised persons. HCoV-NL63 has a capped and polyadenylated ssRNA genome of 27 553 bases in size, with the genome order being 5'-ORF1a-ORF1b-S-ORF3-E-M-N-polyT-3' (Figure 6). Seven distinct ORFs are produced from six distinct mRNAs, which include the full-length genomic RNA and a nested set of five sgRNAs. The five sgRNAs encode for the viral structural and accessory proteins S, ORF3, E, M, and N (Pyrc *et al.*, 2004).
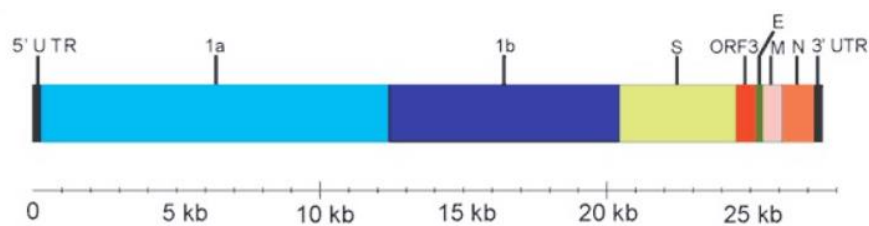

Figure 6. HCoV-NL63 genome organization (adapted from Pyrc *et al.*, 2004).

Unlike other Alphacoronaviruses, which utilize aminopeptidase N to gain access inside cells, HCoV-NL63 exploits the same receptor used by some Betacoronaviruses (including SARS-like CoVs), which is ACE2, a type I membrane protein found in lung, heart, kidneys, and intestine (Hofmann *et al.*, 2005). The HCoV-NL63 receptor ACE2 is a key enzyme of the renin–angiotensin system, which is negatively regulated by ACE2 (Hu *et al.*, 2021).

The first steps of the HCoV-NL63 infection process begins with the virus binding to the cellular membrane via heparan sulfate proteoglycans, which then facilitate interaction with the entry receptor ACE2 (Milewskaa *et al.*, 2018), that is recognized by the viral S protein (Li *et al.*, 2007). A recent study suggested that HCoV-NL63 entry inside cells is mediated by clathrin-mediated endocytosis, as binding of the virus to ACE2 initiates recruitment of clathrin with subsequent formation of clathrin-coated pits. However, the virus can also bypass the endocytic route using TMPRSS2 as the priming protease, enabling entry directly from the cell (Milewskaa *et al.,* 2018).

It was discovered that the N-terminal portion of HCoV-NL63 S protein, corresponding to the receptor-binding domain (RBD), contains a unique 179 amino acids domain that is not

present in other coronaviruses. This domain of the S protein represents the most variable region of the HCoV-NL63 genome and it is supposed to have a role in immune evasion (Hoek *et al.*, 2003; Pyrc *et al.*, 2007). Remarkably, it was found that the HCoV-NL63 S protein has a weaker interaction with ACE2 than the SARS-CoV S protein, and this may partially explain the different pathological consequences of infection by NL63 and SARS-CoV (Mathewson *et al.*, 2008).

1.2 The role of innate immune response during coronavirus infection

Innate immunity is an antigen-nonspecific mechanism used as host's initial defense against foreign and dangerous materials (Turvey and Broide, 2010). Immediate cellular responses to pathogen invasion are crucial for maintaining cell homeostasis and survival for all living organisms (Denney and Ho, 2018). Innate immunity responses rely upon the activity of membrane-bound and cytoplasmic receptors, known as pattern recognition receptors (PRRs), that recognize conserved molecular structures exclusively expressed by microbes, termed pathogen-associated molecular patterns (PAMPs) and damaged-associated molecular patterns (DAMPs), which are molecules released from cells upon inflammation or infection (e.g., uric acid, ROS, heat shock proteins, DNA and RNA). Various PRRs have been discovered until now, including Toll-like receptors (TLRs), nucleotide-binding oligomerization domain-(NOD-) like receptors (NLRs), C-type lectin receptors (CLRs), AIM2-like receptors (ALRs), cyclic GMP-AMP synthase (cGAS), and retinoic acid-inducible gene-(RIG-) I-like receptors (RLRs) (Turvey and Broide, 2010). In mammals, activation of PRRs by PAMPs or DAMPs triggers innate immune responses, producing multiple IFNs and proinflammatory cytokines (Kumar *et al.*, 2011)

Given the nature of their genome, coronaviruses are recognized by RNA sensors, including RLRs and TLRs; in particular, TLR3 and TLR8 are found in endosomal compartments, where they sense single- and double-stranded RNA, respectively. In the cytoplasm, RLRs like RIG-I and melanoma differentiation-associated gene 5 (MDA5) can detect intracellular non-self RNAs possessing specific patterns of secondary structures or biochemical modifications (Figure 7).
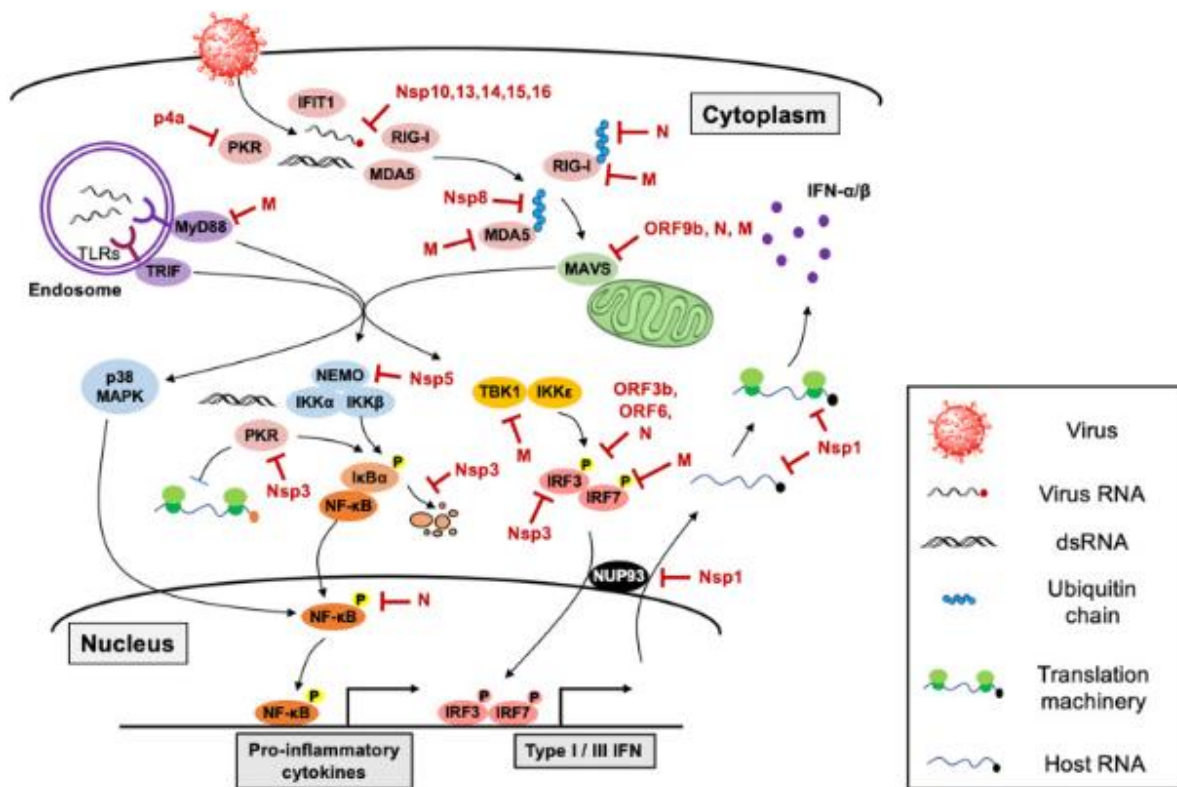
Figure 7. The host innate immune sensing pathway targeted by coronavirus. The multiple host factors in the antiviral signaling cascade are targeted by coronavirus proteins. Innate antiviral sensors can recognize coronavirus invasion by sensing cytosolic or endosomal viral RNA, activation of virus sensors triggers an antiviral signaling cascade to elicit the production of type I or type III IFN as well as proinflammatory cytokines. On the other hand, coronaviruses have evolved multiple strategies to avoid host recognition by impeding the function of antiviral proteins using various viral proteins (adapted from Kasuga *et al*., 2021).

Following interaction with RNA ligands, RLRs and TLRs immediately initiate antiviral defense programs. TLRs initiate downstream signal cascades by recruiting adapter proteins, such as myeloid differentiation primary response 88 (MyD88) (for TLR7 and TLR8) and TIR-domain-containing adapter-inducing IFN-β (TRIF) (for TLR3) (Liu *et al*., 2022). Instead, RLR-mediated signaling starts with the exposure of their caspase activation and recruitment domains (CARDs), through which they bind to the signaling adaptor molecule mitochondria antiviral signaling protein (MAVS). Activated RLRs liberate CARDs to bind MAVS via the CARD-CARD interaction (Seth *et al*., 2005). Adaptor molecules MyD88, TRIF, and MAVS then recruit other ubiquitin ligases, such as TNF receptor-associated factor (TRAF)3 and TRAF6, that associate with antiviral kinases, such as TANK-binding kinase 1 (TBK1), I-kappa-B kinase ε (IKKε), and the IKKα/β/γ complex. Eventually, activation of the transcription factors IRF3, IRF7

and NF-κB leads to the production of type I IFN (IFN-I) and proinflammatory cytokines to operate the host antiviral IFN programs (Kawasaki *et al.*, 2014).

IFN-I response is critical for providing an efficient protection against viral replication. IFN-I production is rapidly triggered by the recognition by host sensors of PAMPs, such as viral nucleic acids (Streicher and Jouvenet, 2019). IFN-I–induced signaling converges on transcription factors, which rapidly induces the expression of hundreds of genes called interferon-stimulated genes (ISGs) (Schneider *et al.*, 2014). ISGs, along with other downstream molecules controlled by IFN-I, including proinflammatory cytokines, have diverse functions, ranging from direct inhibition of viral replication to the recruitment and activation of various immune cells (Crouse *et al.*, 2015). A robust, well-timed, and localized IFN-I response is thus required as a first line of defense against viral infections because it promotes virus clearance, induces tissue repair, and triggers a prolonged adaptive immune response against viruses.

1.2.1 Innate immune evasion of coronaviruses

As already mentioned, a peculiar feature of several coronaviruses, especially those causing severe diseases, is their capacity to evade the immune system. Indeed, different CoV-encoded proteins have been discovered to inhibit multiple steps of the host response as a mean to sustain viral replication and propagation (Li *et al.*, 2021).

Among all immune evasion mechanisms, particularly relevant are those interfering with the initial innate immune response such as RNA sensing, IFN-I production, and signal transducer and activator of transcription (STAT)-1/2 activation, which are shared by SARS-CoV-1/2 and MERS-CoV (Figure 8).
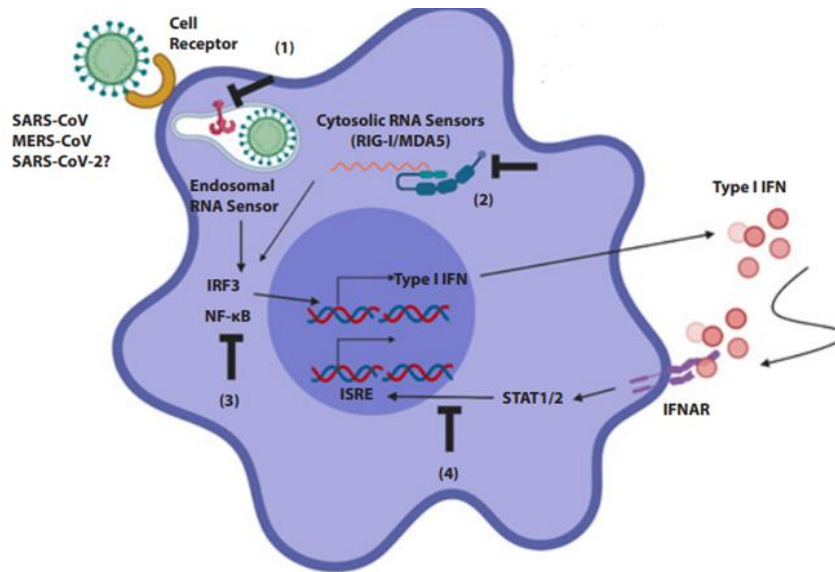
Figure 8. <u>Potential immune evasion mechanisms shared by SARS-CoV, MERS-CoV and SARS-CoV-2</u>. Coronaviruses interfere with multiple steps during initial innate immune responses, including RNA sensing (1 and 2), signaling pathway of INF I production (3), STAT1/2 activation downstream of IFN/IFNAR (4) as indicated by suppressive marks (adapted from Prompetchara *et al*., 2020).

Notably, inhibited, or delayed IFN response is thought to contribute to the pathogenesis of the most severe forms of SARS-CoV-2 infection. Indeed, lack of IFN production in the early stages of infection may impair the correct clearance of the virus, which, on the other hand, continues to replicate undisturbed. As a consequence, high viral titers eventually induce a hyperinflammatory state known as cytokine storm characterized by the presence of huge amounts of proinflammatory cytokines including IL-1, 2, 6, 7, 8, 10, 12, 17 and 18, TNF-α, IFN-γ, granulocyte colony-stimulating factor (G-CSF), and monocyte chemoattractant protein-1 (MCP-1). Overall, this condition determines a strong infiltration of innate and adaptive immune cells within the inflamed tissue, bringing to a possible tissue damage; in addition to this, the systemic inflammation is responsible for the perturbation of coagulation and vascular homeostasis, resulting in capillary leak syndrome, thrombosis, and disseminated intravascular coagulation. All together, these events lead to ARDS, multiorgan failure, and death (Yang *et al*., 2021).

IFN response is mainly antagonized by viral NSPs. For instance, it has been reported that SARS-CoV-2 NSP1 can block phosphorylation and consequent nuclear transport of IRF3, thus impairing the transcription of IFN-I (Kumar *et al*., 2021). Additionally, NSP1 of SARS-CoV-1/2 and MERS-CoV have been confirmed to suppress STAT1/2 phosphorylation and therefore inhibit IFN-mediated signaling (Xia *et al*., 2020). Likewise, SARS-CoV and HCoV-NL63 NSP3, which contains papain-like protease domains (PLPs), has been discovered to suppress IFN-β

16

production by blocking assembly or stability of STING dimers, which are important for downstream signaling (Sun *et al.*, 2012).

Besides NSPs, several viral accessory proteins also contribute to IFN suppression through different mechanisms, including: 1) inhibition of STAT1 phosphorylation by SARS-CoV-2 ORF3a (Xia *et al.*, 2020) and induction of type I IFN receptor (IFNAR1) downregulation by SARS-CoV ORF3a (Minakshi *et al.*, 2009); 2) impairment of nuclear translocation of IRF3 by SARS-CoV-1/2 ORF3b (Konno *et al.*, 2020); and 3) suppression of NF-κB translocation into the nucleus by MERS-CoV ORF4b (Canton *et al.*, 2018).

Another strategy adopted by coronaviruses is to mask viral RNA to prevent it from being recognized by PRRs. As a matter of fact, HCoV have evolved three modes to evade detection by RNA sensors, as 1) exploit double-membrane vesicles to hide nascent viral RNA; 2) mimic eukaryotic mRNAs to shield PAMPs on the viral genome from the recognition; and 3) inhibit the formation of stress granules (SG), which represent an accumulation of viral RNA and viral proteins that provide a pool of substrates for different PRRs such as RIG-I and MDA5 (Li *et al.*, 2021).

1.3   PYHIN protein family

Mammalian cells have evolved sensors of foreign invaders that alert and activate a large variety of antiviral effector proteins. Pyrin and hematopoietic interferon-inducible nuclear (HIN) domain-containing (PYHIN) protein family members have initially been recognized as novel types of PRRs and proposed to trigger innate immune responses and inflammasome activation upon detection of pathogen-derived DNA (Cridland *et al.*, 2012). However, most of the evidence comes from numerous studies on the PYHIN protein AIM2, a cytoplasmic sensor of double-stranded DNAs. In contrast to AIM2, however, the remaining human PYHIN proteins are predominantly localized in the nucleus and accumulating evidence suggests that they exert antiviral effects by suppressing viral transcription rather than by sensing viral DNAs (Schattgen and Fitzgerald, 2011).

PYHIN proteins are characterized by two functional domains: an N-terminal pyrin domain (PYD) and at least one C-terminal hematopoietic interferon-inducible nuclear protein, with a 200-amino-acid repeat domain (HIN200). The PYD is part of the bigger superfamily of death domains (DD) characterized by an alpha-helical-based folding, promoting homo- or hetero-typic interactions with other PYD-containing proteins. PYD-PYD interactions regulate a variety

of cellular processes, ranging from inflammation and immunity to apoptosis and cell cycle (Stehlik, 2007).

The HIN domain is only found in PYHIN family members and promotes DNA-binding in a non-sequence specific fashion via tandem oligonucleotide/oligosaccharide-binding (OB) folds (Shaw and Liu, 2014). Sequence independent DNA binding is achieved by electrostatic interactions between specific side chains of positively charged HIN domain amino acid residues and the phosphate groups in the DNA backbone (Jin *et al*., 2012). HIN domains have been classified in three subfamilies, designated -A, -B, and -C, based on the amino acidic sequence following a conserved MFHATVAT motif (Ludlow *et al*., 2005) (Figure 9).
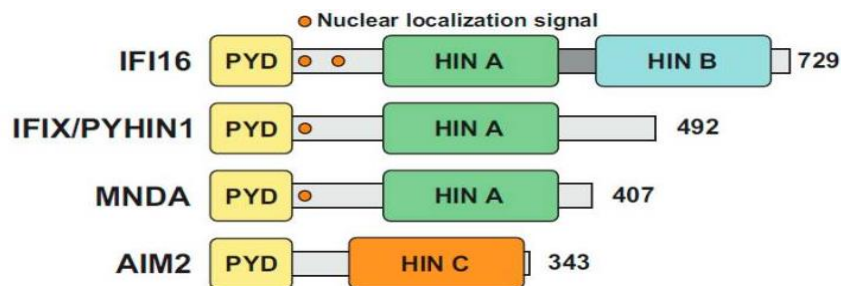

Figure 9. <u>**The human pyrin and hematopoietic interferon-inducible nuclear (HIN) domain (PYHIN) protein family.**</u> Schematic organization of human PYHIN proteins. Each PYHIN family member possesses an N-terminal pyrin domain (PYD) and one or more HIN domains, classified as HIN A, HIN B and HIN C. With the exception of AIM2, all PYHIN proteins harbor at least one nuclear localization signal (NLS) (adapted from Bosso and Kirchhoff, 2020).

PYHIN coding genes are exclusively found in mammals and their numbers range from 1 in horses to up to 13 in mice (Cridland *et al*.,2012). Humans encode four PYHIN proteins: IFN-γ-Inducible protein 16 (IFI16), IFN-Inducible protein X (IFIX) also known as Pyrin and HIN domain-containing protein 1 (PYHIN1), Myeloid Nuclear Differentiation Antigen (MNDA), and Absent in Melanoma 2 (AIM2) (Connolly and Bowie, 2014).

The best characterized member of the human PYHIN family is AIM2, which is normally localized in the cytoplasm, where it acts as a sensor of cytosolic dsDNA; upon interaction with dsDNA, AIM2 activates a cascade of events that eventually leads to formation of caspase-1-activating inflammasome, production of pro-inflammatory cytokines (IL-18, IL-1β) and apoptotic cell death.

Likewise, pathogen-derived nucleic acids may be also recognized by IFI16 in both nucleus and cytoplasm. Indeed, it has been suggested that the lightly packed form of foreign DNA entering the nucleus may allow IFI16 to distinguish it from the densely packed cellular DNA.

In addition, it has been reported that after infection by different viruses, IFI16 translocate to the cytosol and cooperates with the cyclic guanosine monophosphate-adenosine monophosphate (cGAMP) synthase (cGAS) to activate STING, which in turn activates IFN transcription (Bosso *et al.*, 2020)

Besides their function as innate DNA sensors, there is now much evidence that PYHIN proteins are also capable of inhibiting viral pathogens serving as antiviral restriction factors. In particular, IFI16 has been proven able to suppress viral transcription of herpes-, retro-, papilloma-, cytomegalovirus and hepatitis viruses through various mechanisms, including epigenetic modifications and interference with the transcription factor Sp1 (Bosso and Kirchhoff, 2020).

Intriguingly, bats harbor genetic or functional loss of a number of proteins involved in host innate immunity, including the PYHIN gene family that comprises the interferon-inducible gene IFI16 (Zhang *et al.*, 2012; Ahn *et al.*, 2016). It has been hypothesized that genetic changes including the loss of the PYHIN locus occurred in response to the unique capacity of bats to fly great distances. Indeed, bat immune system has evolved overtime to limit excessive inflammation derived from the high metabolic demand of flight, which is responsible for the release of huge amounts of reactive oxygen species (ROS), damaged DNA and other danger signals that are known to trigger inflammasome activation. At the same time, these alterations have contributed to create a state of tolerance in bats against a number of deadly viruses, including filoviruses (Ebola and Marburg), paramyxoviruses (Hendra and Nipah), and severe acute respiratory syndrome-like coronaviruses (SARS-CoV, MERS-CoV, and SARS-CoV-2) (Luis *et al.*, 2013). Due to this state of tolerance, infected bats show no or minimal signs of disease even in presence of high viral titers either in tissue or sera, although the same viruses frequently cause aberrant innate immune responses in humans (Irving *et al.*, 2021).

As PYHIN proteins have been shown to restrict viral replication through different mechanisms, the loss of the entire PYHIN locus may explain the abundance of viruses detected in bats. Furthermore, although bats contain other cytosolic DNA immune sensors, the PYHIN family is the only class able to drive inflammasomes activation, which, among their many functions, also have a role in controlling the mass-inflammatory response to invading pathogens. Therefore, PYHIN deletion may also play a role in asymptomaticity of bats to most of the viruses (Ahn *et al.*, 2016).

1.3.1 Interferon – gamma - Inducible protein 16

IFI16 is a member of the PYHIN-containing protein family, which encodes a class of homologous proteins that share a 200-amino acid signature motif (HIN) (Miyanaga *et al.*, 2001).

Structurally, IFI16 is composed by two HIN domains (A and B) separated by a spacer region. These domains allow IFI16 to interact with both dsDNA and ssDNA, and with RNA, in a sequence-independent manner (Unterholzner *et al.*, 2011; Jiang *et al.*, 2021). In addition, IFI16 possesses a N-terminal PYRIN domain which enables protein-protein interactions (Figure 10) (Dell'Oste *et al.*, 2015).
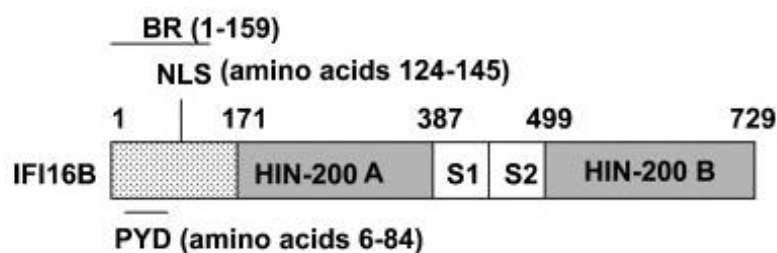

Figure 10. <u>Schematic representation of structural and functional domains in IFI16 protein</u>. Light dotted area in the amino terminus includes the basic region (BR; amino acid residues 1-159), which is sufficient to bind dsDNA in vitro, a PYD domain (amino acid residues 6-84), and a nuclear localization signal (NLS; amino acid residues 124-145). The dark gray boxes in the IFI16 protein denote a type-A and a type-B 200-AA repeat (or HIN-200 domain), respectively. White boxes (the S1 and S2) between the two repeats denote two spacer regions in the IFI16B protein (adapted from Dell'Oste *et al.*, 2015).

As it contains a nuclear localization signal (NLS), IFI16 was originally labelled as nuclear protein. However, there is now evidence that IFI16 can also be detected in the cytoplasm of cells, even though molecular mechanisms regulating IFI16 redistribution between nuclear and cytosolic compartments are only partially understood (Dell'Oste *et al.*, 2015). For example, nucleus-to-cytoplasm translocation of IFI16 was observed in keratinocytes upon exposure to UVB (Costa *et al.*, 2011); likewise, IFI16 moves to the cytoplasm during infection of different viruses such as Epstein-Barr virus (EBV), herpesvirus type 1 (HSV-1), and cytomegalovirus (CMV) (Dell'Oste *et al.*, 2014). Furthermore, it was found that upon infection with Kaposi Sarcoma herpesvirus (KSHV), IFI16, along with ASC and procaspase 1, redistribute to the cytoplasm to form a functional inflammasome, leading to caspase 1 activation and IL-1β cleavage (Zheng *et al.*, 2020).

The role of IFI16 in sensing DNA viruses is well-characterized, but its function during RNA virus infections remains partially unknown. A recent study showed that IFI16 could inhibit influenza A virus (IAV) replication in cooperation with RIG-I (Jiang *et al.*, 2021). RIG-I is a member of the RLRs family and serves as a cytoplasmic sensor of PAMPs for RNA viruses. RIG-I activation induces an intracellular immune response characterized by IFN-I production and antiviral gene expression aimed at controlling virus infection (Loo and Gale, 2011). According to the recent study, IFI16 can enhance the transcription of RIG-I during IAV infection and interact with RIG-I protein, thereby increasing the sensitivity of RIG-I signaling (Jiang *et al.*, 2021). Moreover, it was shown that IFI16 expression is upregulated following IAV infection and can directly interact with the viral RNA genome (Jiang *et al.*, 2021). Another study also reported the ability of IFI16 to induce pyroptosis in alveolar epithelial cells infected by IAV as to suppress cell-to-cell viral transmission. Although precise mechanisms are still unknown, it is thought that IFI16-induced programmed cell death starts with the interaction between IFI16 and viral RNA, which predominantly occurs in the nucleus (Mishra *et al.*, 2022).

IFI16 was also found able to inhibit replication of other RNA viruses. For instance, IFI16 directly interacts with chikungunya virus (CHIKV) genomic RNA and inhibits its replication and maturation by acting as an antiviral restriction factor (Kim *et al.*, 2020). Also, IFI16 can efficiently restrict the replication of porcine reproductive and respiratory syndrome virus 2 (PPRSV-2) by directly binding MAVS and promoting MAVS-mediated IFN-I production (Chang *et al.*, 2019).

2. AIM OF THE WORK

Due to their ability to fly great distances, the immune system of bats has adapted overtime to limit collateral damage caused by by-products of elevated metabolic rate (Zhang *et al*., 2012).

These changes have contributed to make bats ideal reservoir hosts for a great variety of zoonotic viruses, including Coronaviruses (Luis *et al*., 2013). The reason why bats are tolerant to these viral infections could be explained by the fact that they have an impaired interferon (IFN) response, due to a mutation in the STING protein (Xie *et al*., 2018). In addition, genomic analysis revealed that the entire pyrin and HIN domain (PYHIN)-containing protein family is lost in bats. This protein family encompasses sensors of intracellular self and foreign DNA and activators of the inflammasome and IFN response (Ahn *et al*., 2016). Among these proteins, the Interferon-γ-Inducible protein 16 (IFI16) plays a role in the innate immune response by acting as a DNA sensor in inflammasome signaling and as viral restriction factor (Bawadekar *et al*., 2015). Although IFI16 has been better characterised in the context of DNA viruses, several studies also demonstrated an antagonizing role of IFI16 against some RNA viruses, including IAV (Jiang *et al*., 2021), CHIKV (Kim *et al*., 2020), and PPRSV-2 (Chang *et al*., 2019).

Despite the emerging evidence of IFI16 playing crucial role in the control of RNA virus replication, it remains unclear whether IFI16 interacts or interferes with coronavirus replication. According to this background, we decided to investigate whether IFI16 is also a key regulator of the host response to human coronavirus (HCoV) infection, and that therapeutic modulation of this pathway may impact HCoV replication/infectivity.

To this aim, we decided to work with HCoV-NL63, an Alphacoronavirus associated with a low pathogenicity that exploits ACE2 receptor to gain access into cells and represents a good prototype of HCoVs. We characterized NL63 infection in a gold-standard cell line, namely LLC-MK2, a rhesus macaque epithelial kidney cell line that supports efficient replication of NL63.

The studies described in this thesis aimed at understanding the molecular events involving IFI16 in HCoV sensing and characterizing the host response, as well as the signaling pathways triggered by IFI16-mediated sensing of HCoVs.

3. MATERIALS AND METHODS

3.1 Cell lines and viruses

Experiments were performed on rhesus monkey kidney LLC-MK2 (ATCC: CCL-7) cells. Dulbecco's Modified Eagle's Medium (DMEM) was used as a culture media for all the cells along with additional supplements, i.e., 10% fetal bovine serum (FBS), 100 U/ml penicillin (P), 100 µg/ml of streptomycin (S) and 0.05mM glutamine (G) as supplements.

The human coronavirus strain NL63 (HCoV-NL63) (NR-470, also referred to as Amsterdam I, Bei Resources) was kindly provided by Lucia Nencioni (University of Rome, La Sapienza, Rome, Italy). HCoV-NL63 was proliferated in LLC-MK2 and Caco-2 cells at 34 °C in a humidified 5% CO_2 incubator and titrated by the standard plaque assay method on LLC-MK2 cells, as described later.

3.2 HCoV-NL63 production

HCoV-NL63 was generated by infecting monolayers of LLC-MK2 cells, at multiplicity of infection (MOI) 0.01. The flasks were incubated at 34°C, 5% CO2, and harvested on day 5-6 when cytopathic effect (CPE) was visible. For harvesting, flasks were frozen at -80°C and thawed. Cells and supernatant were centrifuged for 10 min at 1500rpm. Cleared supernatant was aliquoted and stored at -80°C. The virus yield was assessed by titration on fully confluent LLC-MK2 cells in 96-well plates.

3.3 HCoV-NL63 titration

Briefly, LLC-MK2 cells were seeded 1 day before infection in 96-well plates, reaching confluency at the time of infection. The viral suspension was serially diluted in DMEM supplemented with 10% fetal bovine serum and inoculated; the infected wells were centrifuged at 2000 rpm for 30 minutes and then incubated at 34 °C for 2 h, allowing viruses to attach and enter the cells. After this time, cells were washed with medium, and overlaid with 0.8% methylcellulose. The plates were incubated at 34°C and 5% CO_2. Overlays were removed on day 6 and stained with a 0.2% crystal violet solution and plaques are counted using a light microscope. Viral titers were expressed in terms of plaque forming units per ml (PFU/ml).

3.4 HCoV-NL63 infection

Subconfluent LLC-MK2 cells cells were infected with the appropriate MOI and virus absorption was allowed for 2-8 hours before changing media. Every infection with HCoV-NL63

was performed at MOI 1 and 5% CO_2. For the kinetics, at 5 dpi supernatants were collected, centrifuged at 2000 rpm for 5 minutes and stored at -80°C.

3.5 RNA extraction and quantification

For gene expression analysis, cells were treated with 500 μL TRIzol Reagent, which disrupts cells and cells components without altering RNA's integrity during homogenization, and were incubated at room temperature for 10 min. After, 100 μL of chloroform (chloroform: TRIzol 1:5) was added in each sample and cells were incubated at room temperature for 10 min. Samples were centrifuged at 12000g for 15 min at 4°C to allow separation of solutions' aqueous and organic phases containing RNA and protein, respectively. The upper transparent phase (corresponding to RNA) was recovered and 250 μL of isopropanol (isopropanol: TRIzol 1:2) was added in each sample. Samples were resuspended, incubated for 10 min at room temperature, and then centrifuged at 12000 for 10 min at 4°C to allow RNA precipitation. Once the supernatants were removed, RNA pellets were washed with 500 μL 70% ethanol, and centrifuged at 7500g for 5 min at 4°C. After supernatants were removed, pellets were left to dry, and finally were resuspended in 15 μL nuclease-free water.

The average concentration of RNA present in each sample was determined by using the *ThermoScientific NanoDrop spectrophotometer*. The photometric measurement of nucleic acids is based on the intrinsic absorptivity properties of DNA or RNA; when an absorption spectrum is measured, nucleic acids absorb light with a characteristic peak at 260 nm. The signal is measured by the spectrophotometer and expressed as absorbance values of the sample. To perform RNA quantification, initially a blank (1 μL distilled water) was run, followed by 1 μL of each sample. Absorbance values of each sample were converted by the software in RNA concentration, measured in ng/μL.

3.6 DNase treatment and retro transcription

For removal of genomic DNA, RNA extracts were treated using the *TURBO DNA-free™ Kit* according to manufacturer's instruction (Invitrogen).

For cDNA synthesis, *SensiFAST cDNA Synthesis Kit* was used according to manufacturer's instruction (Meridian Bioscience). The total RNA of each sample was mixed with 4 μL 5X TransAmp Buffer and 1 μL Reverse Transcriptase; DNase/RNase free water was used to reach the final volume of 20 μL. Reverse transcription was performed by using the *C1000 Touch Thermal Cycler* (Bio-Rad Laboratories). The conditions used for retro transcription were the following: 25 °C for 10 min, 42 °C for 15 min, 85 °C for 5 min.

3.7 Real-Time qPCR

The viral cDNA (1 µL per sample) was amplified in a 20 µL reaction mixture containing 10 µL SensiFast SYBR (Bioline) 1 µL forward primer, 1 µL reverse primer, and 7 µL water. Primers used for qPCR assay were the following: *NL63 N gene* (For: AGGACC TTAAATTCAGACAACGTTCT; Rev: GATTACGTTTGCGATTACCAAGACT), *GAPDH* (For: TCACCACCATGGAGAAGGC; Rev: GCTAAGCAGTTGGTGGTGCA), *NL63 ORF1ab* (For: TGTTGTAGTAGGTGGTTGTGTAACATCT; Rev: AATTTTTGT GCACCAGTATCAAGTTT), *subgenomic NL63 N gene* (For: TAAAGAATTTTTCTATCT ATAGATAG; Rev: TACGCCAACGCTCTTGAAC), *subgenomic NL63 S gene* (For: TAA AGAATTTTTCTATCTATAGATAG; Rev: TATGGAGCGCAAAAGCAC). The reaction conditions consisted of an enzyme activation cycle of 30 s at 95°C, 40 cycles of 10 s of denaturation at 95°C, and 10 s of annealing at 60°C.

The conditions used for the amplification of subgenomic mRNAs were the following: 3 min at 95°C, 40 cycles of 30 s at 95°C, 30 s at 47°C, and 25 s at 72°C, followed by 5 min at 72°C and 10 min at 4°C. The PCR products were run on 1% agarose gels (1X Tris-acetate EDTA [TAE] Buffer) and visualized using *ChemiDoc Touch Imaging System* (Bio-Rad).

3.8 Protein extraction and quantification

Whole-cell protein extracts were obtained using 100 µL cell lysis buffer containing 150 mM NaCl, 50 mM Tris-HCl pH 8, 1% NP40, 0,5% sodium deoxycholate, 0,1% SDS, with the addition of protease inhibitors (25 µL/mL, Sigma-Aldrich). The samples were homogenized for 1 hour at 4°C under rotation and then centrifuged at 14000g for 10 min at 4°C. The supernatant was collected in a micro-centrifuge tube and quantified. Protein concentration was determined using Bradford Protein Assay based on an absorbance shift of the dye Coomassie Brilliant Blue G-250. In an acidic environment, the red form of the dye is converted into its blue form, binding to the protein being assayed. The protein-dye complex causes a spectral shift in the maximum absorption of the dye from 465 to 595 nm. The increase of absorbance at 595 nm is proportional to the amount of bound dye, and thus to the concentration of protein present in the sample. Bovine serum albumin (BSA) was used to calibrate the assay by preparing six serial dilutions of protein diluted with PBS1X to final concentrations of 1, 2.5, 5, 10, 15, 30 µg/µL (2 µL of cell lysis Buffer were added in each dilution). Test tubes were prepared by adding 2 µL sample, 498 µL PBS, and 500 µL Bradford Reagent; 2 blanks were obtained by adding 498 µL PBS, 2 µL RIPA Buffer, and 500 µL Bradford Reagent. Absorbance readings were

measured at 595 nm using a spectrophotometer and the standard curve was used to provide a relative measurement of protein concentration of each sample.

3.9 Western Blot

For protein analysis, protein extracts were dissolved in *Laemmli Sample Buffer 4X* (0.02% bromophenol blue, 8% β-mercaptoethanol, 250mM-HCl, 8% SDS, 40% Glycerol) and heated at 95°C for 5 min thus leading to denaturation of proteins.

Proteins were separated by their molecular weight under denaturing conditions using ReadyGels (7.5%; Bio-Rad). The samples (20 μL) and a molecular weight ladder (7 μL) were loaded into appropriate wells; gels were initially run at 80V until complete separation of the marker's bands, and then at 200V. Proteins were transferred from the SDS-polyacrylamide gels to nitrocellulose membranes by using *Trans-blot Turbo Blotting System* according to manufacturer's instruction (Bio-Rad). In order to confirm the transfer, membranes were stained with Ponceau stain. To visualize the proteins, membranes were washed three times with TBS-T 1X (10mM Tris-HCl, pH 7.5, 100mM NaCl, 0.1% Tween-20). To minimize any unspecific interaction of the antibody, membranes were blocked in 10% non-fat dry milk dissolved in TBS-T 1X for 1 hour, followed by incubation with primary antibodies for 2 hours at room temperature on a rocker; primary antibodies used for the experiments are listed in the table on *chapter 3.11*. Thereafter, membranes were washed three times in TBS-T 1X to eliminate unbound antibody residues and subsequently incubated with the respective species-specific secondary antibody (Anti-rabbit diluted 1:2000; Anti-mouse diluted 1:4000). Proteins were detected using the instrument *ChemiDoc Touch Imaging System* (Bio-Rad). Images were acquired, and densitometry of the bands was performed using Image Labsoftware (Bio-Rad Laboratories Srl).

3.10 Immunofluorescence

For immunofluorescence analysis, cells were fixed with 4% paraformaldehyde (PAF) for 10 min at room temperature. To enable antibodies to cross the cellular membranes, permeabilization was performed with 0.5% Triton X-100 in PBS 1X for 20 min on ice. After, to reduce unspecific binding of antibodies to non-target structures, blocking was performed with 1% Normal Goat Serum (NGS) in PBS 1X for 30 min at room temperature. This was followed by 1 hour incubation with the primary antibody diluted in blocking solution. After, several washings were performed with PBS 1X + 0.05% Tween-20 to remove the unbound antibody,

and then 1-hour incubation with secondary antibody in the dark was performed; in addition, 4',6-diamidino-2-phenylindole (DAPI) was added to stain cells' nuclei. After few washes, coverslips were mounted on slides using anti-fade mounting medium and visualized using the Multiphoton Microscope Leica TCS SP8 (Leica Microsystems, Wetzlar, Germany), while images were processed using the Leica Application Suite X (LAS X).

3.11 Antibodies

Antibody (Company name, location)	Dilution Western Blot	Dilution IF
Rabbit MAb anti-RIG-I (*Millipore*)	1:1000	
Mouse MAb anti-IFI16 (Santa-Cruz)	1:1000	1:600
Rabbit PAb anti-IFI16 (*in-house made*)	1:1000	1:200
Rabbit MAb anti-NL63 NP (*Sino Biological*)	1:2000	1:200
Mouse MAb anti-GAPDH (*Proteintech*)	1:10000	

3.12 Statistical analysis

All statistical tests were performed using Graph-Pad Prism version 7.00 for Windows (GraphPad Software). The data are presented as mean ± standard deviation (SD). For comparisons consisting of two or more groups, means were compared using two tailed Student's t tests or one-way ANOVA followed by Bonferroni's posttests. Differences were considered statistically significant at a P value of < 0.05.

4.RESULTS

4.1 Kinetics of HCoV-NL63 infection and innate response in LLC-MK2 cells

To understand the role of the innate immune sensor IFI16 in controlling HCoV replication, we decided to work with the Alpha-HCoV-NL63, which is a good prototype of HCoVs and due to its low pathogenicity, it can be handled in BSL2 laboratories available in our institution.

Given the limited number of studies regarding NL63, we began our experiments by characterizing NL63 infection in a gold-standard cell line. For this purpose, we decided to use the monkey kidney-derived epithelial cell line LLC-MK2, which produce a visible cytopathic effect upon NL63 infection and is often used for viral production (Herzog *et al*., 2008)

At first, to investigate the kinetic of NL63 infection, we measured by RT-qPCR genomic and subgenomic mRNA levels in LLC-MK2 cells infected with NL63 at MOI 1 (Figure 11)**.** In detail, we used a specific pair of primers detecting: 1) only viral genomic RNA ORF1ab, 2) both the viral genome and subgenomic mRNAs N, then 3) only the subgenomic N and S mRNA levels. According, to the literature, NL63 has a long viral cycle (Herzog *et al*., 2008), thus its kinetic was analyzed from 2 hpi to 6 dpi.
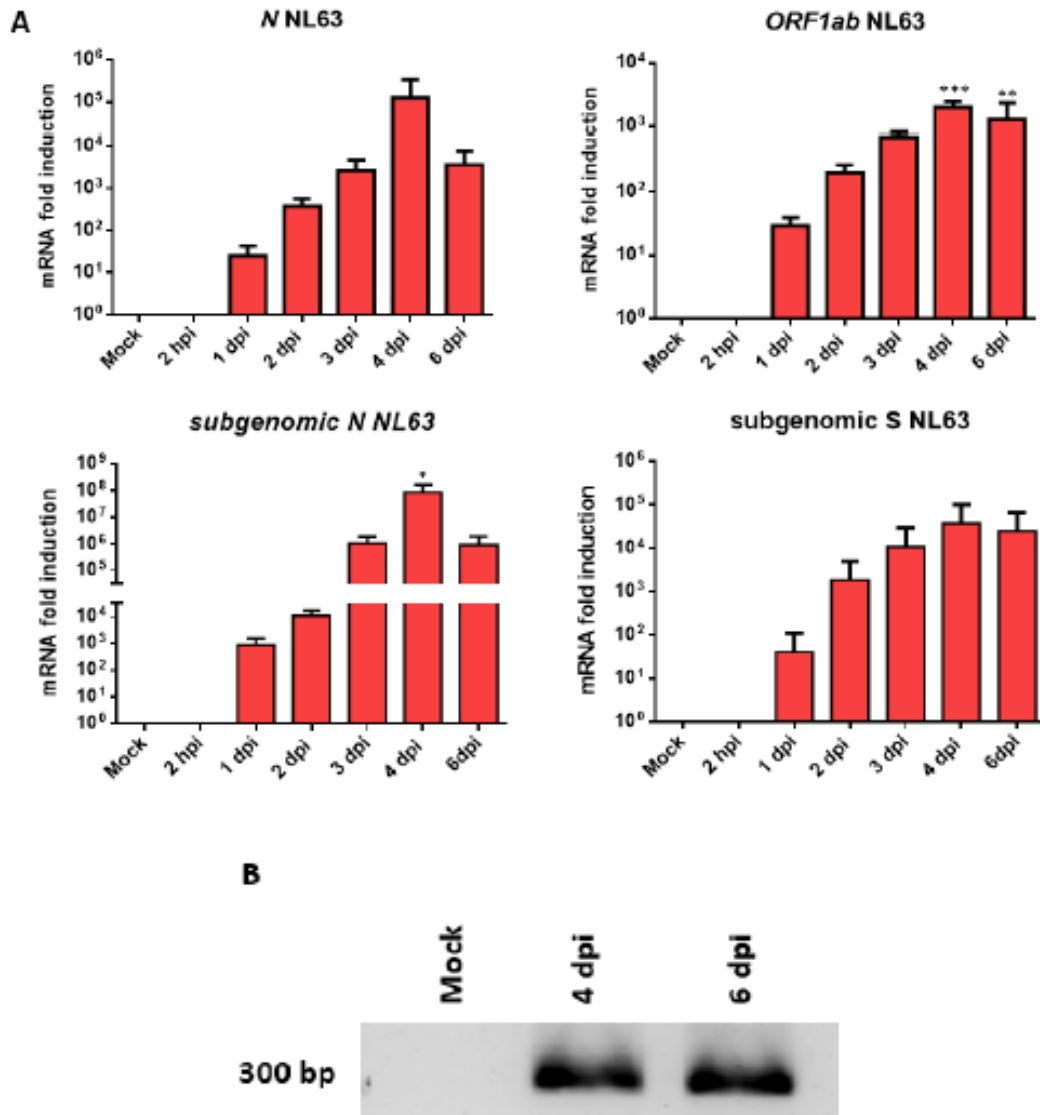
Figure 11. <u>Virus RNA levels in LLC-MK2 cells infected with HCoV-NL63</u>. (**A**) LLC-MK2 cells were infected with NL63 MOI 1 and at the indicated time points, total RNA was isolated from cells and virus RNA levels were determined by means of RT-qPCR, with N specific primers detecting both genomic and subgenomic mRNAs (A left panel), with ORF1ab specific primers detecting only the viral RNA genome (A right panel), with primers detecting only subgenomic N and S mRNAs (B left and right panel, respectively). Graphs show the average fold change and SD for each time-point compared to the 2 h time-point. Intracellular viral RNA levels were corrected for total cell numbers using GAPDH as a standard. Bars represent the means and S*D* from three independent experiments (*p <0.05, **p <0.01, ***p <0.001, one-way ANOVA followed by Bonferroni's posttests, for comparison of infected vs mock cells). (**B**) PCR products were run on 1% agarose gels (1X Tris-acetate EDTA [TAE] Buffer) and visualized using ChemiDoc Touch Imaging System (Bio-Rad). Positions of nucleotide size markers are shown on the left side of the panel. The figure shows a band in infected cells, corresponding to the N gene, at both 4 and 6 dpi, whereas in mock cells the same band is absent.

The results showed that the viral mRNA levels encoding for N protein started to increase from 1 dpi, reaching a peak at 4 dpi with a 100.000-fold induction compared to levels observed at 2 hpi. In agreement with these data, genomic ORF1ab RNA levels started to rise up at 1 dpi, peaking at 4 dpi with a 1.000-fold induction. Similarly, also the transcription initiated at 1 dpi with a peak at 4 dpi for both subgenomic N and S proteins, with a higher induction of N (10^8) compared to S (10^4-10^5)

To further confirm our findings, PCR products of the sgmRNA levels were run on agarose gel to evaluate the correct amplification of this segment (Figure 11B), through which we verified the presence of a clear band at 300 bp (corresponding to the N sgmRNA) in infected cells at both 4 dpi and 6 dpi. As expected, the same band was absent in mock cells. Supernatants of LLC-MK2 cells infected with NL63 at MOI 1 were then collected at 5 dpi to perform viral titration by standard plaque assay, through which we were able to demonstrate a viral titer of approximately 4 x 10^3 PFU/ml (Figure 12).
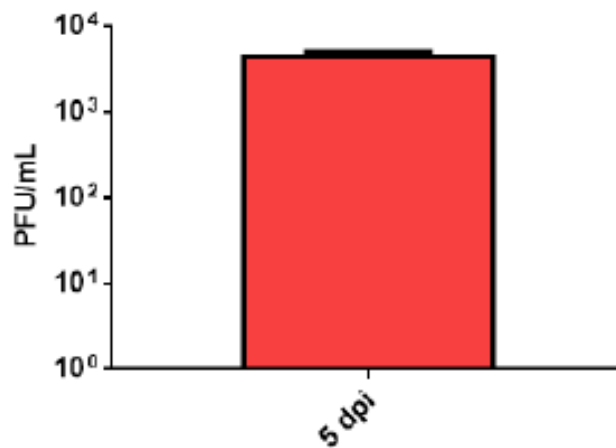

Figure 12. <u>NL63 titration in LLC-MK2 cells infected at MOI 1</u>. Plaque assay was performed on supernatants collected from LLC-MK2 cells at 5 dpi following the procedure already described in chapter 3.3.

We also investigated NP and IFI16 protein expression by western blot analysis (Figure 13). This assay confirmed that NP progressively increased during viral infection and reached its peak approximately at 3 dpi. We also demonstrated that NL63 infection does not modulate the levels of the innate immune sensor IFI16.
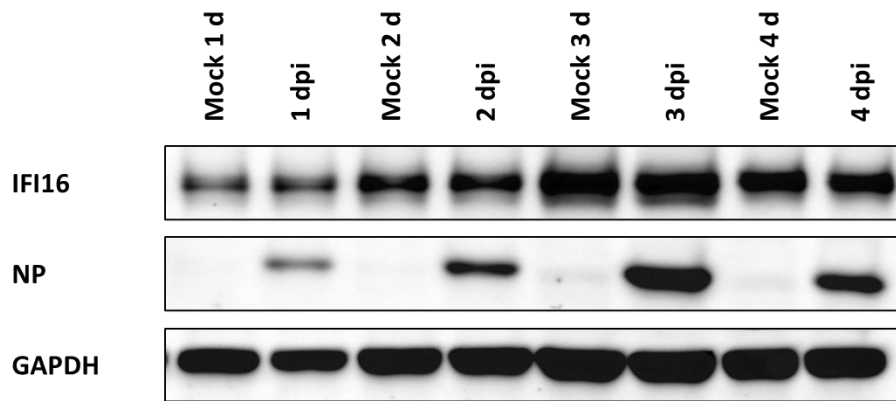

Figure 13. <u>**Protein expression of NP and IFI16 in LLC-MK2 upon NL63 infection**</u>. Cellular extracts from LLC-MK2 cells infected with NL63 at MOI 1 were collected at 1 dpi, 2 dpi, 3 dpi, 4 dpi, to evaluate NP and IFI16 expression. The housekeeping gene GAPDH was used as loading control for protein normalization.

To complete the characterization of NL63 infection in LLC-MK2, we wanted to determine whether LLC-MK2 cells were capable of inducing an immune response upon NL63 infection. With this aim, we used real-time qPCR analysis to evaluate the expression of *IFN-β* and *IFN-λ1*, as well as that of two IFN-inducible genes, namely, *Mx1* and *Mx2*. In Figure 14 is shown that there is no induction of *IFN-β* neither *IFN-λ1* upon infection, indeed mRNA levels of *Mx1* and *Mx2* were not affected as well, indicating that LLC-MK2 cells do not mount any IFN response to NL63 infection.
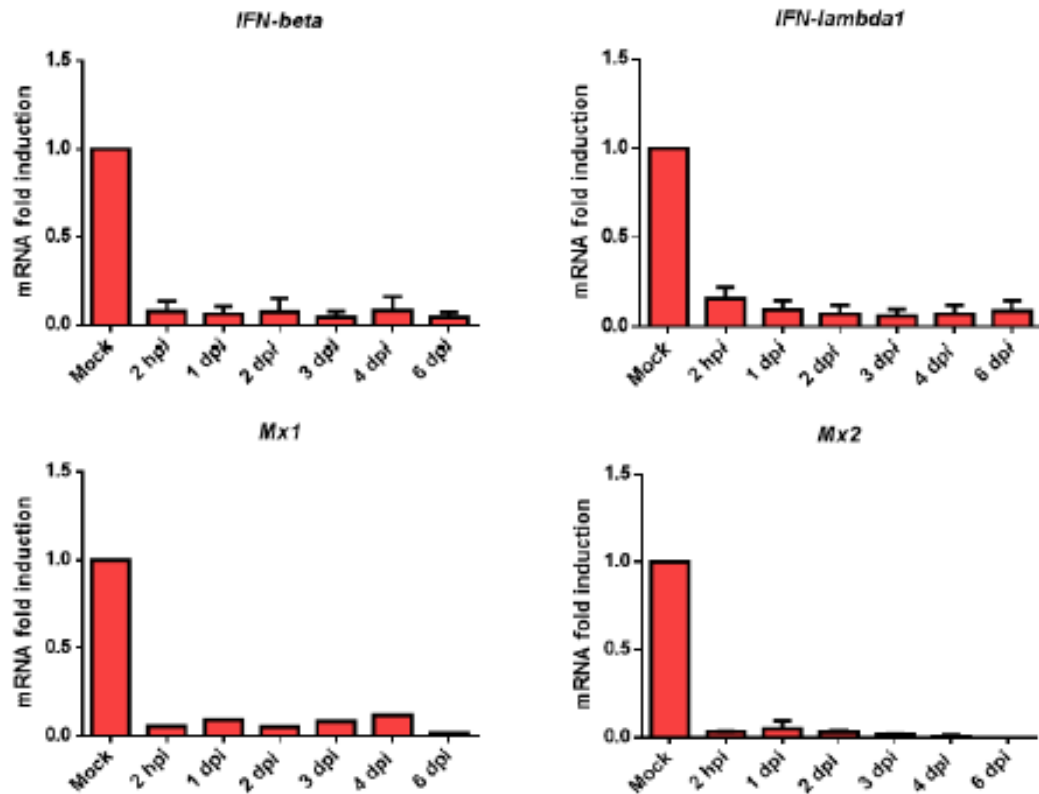
Figure 14. <u>NL63 does not elicit an IFN response in LLC-MK2 cells</u>. Cell lysates were obtained from LLC-MK2 cells infected with NL63 MOI 1 at the indicated time points. Total RNA was isolated from cells and IFN-β, IFN-λ1, Mx1, and Mx2 levels were detected by Real-time qPCR. Values were normalized to the housekeeping GAPDH gene mRNA and plotted as fold induction relative to mock-infected LLC-MK2 (set at 1). Bars show means and SD from three independent experiments.

4.2 IFI16 binds HCoV-NL63 nucleoprotein

HCoVs replicate in the cytoplasm by forming double-membrane structures named replication organelles (ROs) that protect viral RNA from degradation and detection by host cellular immune sensors (Roingeard *et al*., 2022). Given that IFI16 can bind to RNA viral genomes (Jiang*et al.*, 2021; Kim *et al*., 2020), we asked whether IFI16 could form a complex with NP, which is localized in the cytoplasm and can bind to the viral genome.

To this aim, we performed an immunofluorescence analysis to assess IFI16 localization upon coronavirus infection; thus, we infected LLC-MK2 cells with NL63 at MOI 1 and performed co-staining experiments using antibodies directed against IFI16 and the viral protein NP. We observed that IFI16 was predominantly nuclear under basal conditions, but it is massively translocated to cytoplasm and co-localized with NP at 3 dpi (Figure 15).
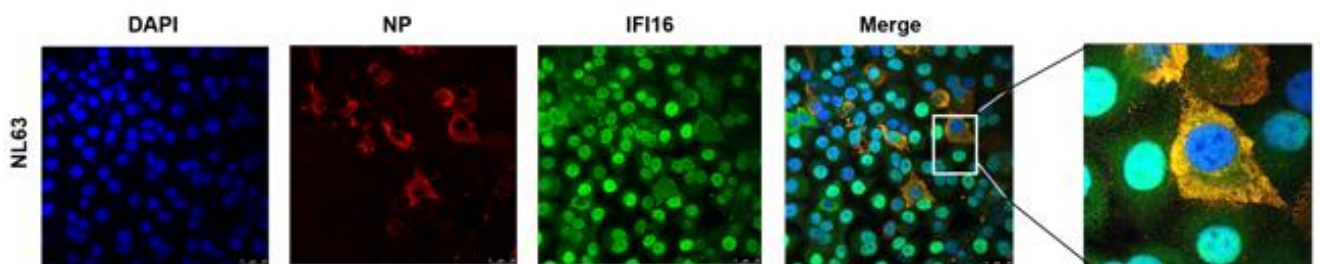

Figure 15. <u>Nuclear translocation of IFI16 upon coronavirus infection</u>. Immunofluorescence analysis of NL63-infected LLC-MK2 cells (MOI 1). Cells were stained with antibodies against NP and IFI16 at 3 dpi.

After finding that IFI16 translocated from the nucleus to the cytoplasm and colocalized with the NP protein upon infection, we asked whether the two proteins interacted. To this end, LLC-MK2 cells were infected with NL63 at MOI 1, and total cell extracts were collected at 3 dpi to run the immunoprecipitation assay. As shown in Figure 16, the NP protein coimmunoprecipitates with the IFI16 protein in NL63-infected LLC-MK2-cells.
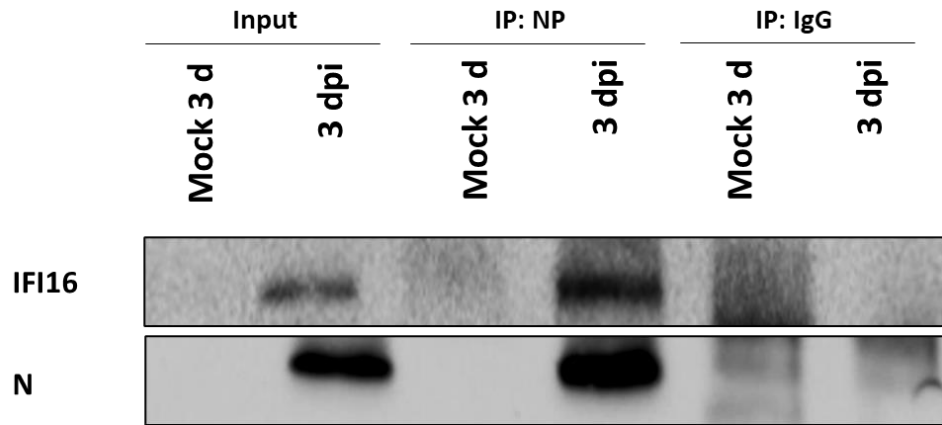
Figure 16. IFI16 binds to viral nucleoprotein. Cell lysates from NL63-infected LLC-MK2 cells were harvested at 3 dpi and immunoprecipitated for viral NP. WB was performed to check IFI16 binding to the immunoprecipitated NP using antibodies against IFI16 and NP. Input is a non-immunoprecipitated sample as a positive control, and IgG is a control.

4.3 HCoV-NL63 infection in transfected control and IFI16 knock-out LLC-MK2 cells

To gain more insight into the impact of IFI16 on HCoV replication and innate immune response, we assessed NL63 infection in transfected control (TC) and IFI16 knock-out (KO) LLC-MK2 cells. To this aim, we obtained two clones of LLC-MK2 whereby the IFI16 gene has been stably knocked down, using the CRISPR-Cas9 gene editing technology (Figure 17). Importantly, we performed the experiments only on one clone of the two and considering the three main time points of NL63 kinetic (1 dpi, 3 dpi and 6 dpi).
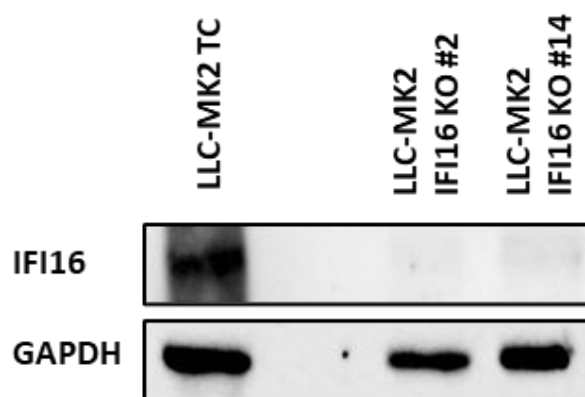

Figure 17. IFI16 expression in TC and IFI16 KO LLC-MK2 cells. Cellular extracts were collected at 3 dpi from TC and IFI16 KO LLC-MK2 cells infected with NL63 (MOI 1). The housekeeping gene GAPDH was used as loading control for protein normalization.

Firstly, we wanted to investigate NL63 infection and kinetic in the absence of IFI16, thus we performed a real-time qPCR analysis to check the levels of the genomic RNA ORF1ab, and the subgenomic N and S mRNAs in TC and IFI16 KO LLC-MK2 cells, both infected with NL63 at MOI 1.The RNA levels of ORF1ab suggest that in absence of IFI16, the replication of NL63 is slightly reduced at 1 dpi and 3 dpi, whereas it is halved at 6 dpi. The N and S transcripts are very much decreased, indicating a lowering of viral transcription when IFI16 is not present (Figure 18).
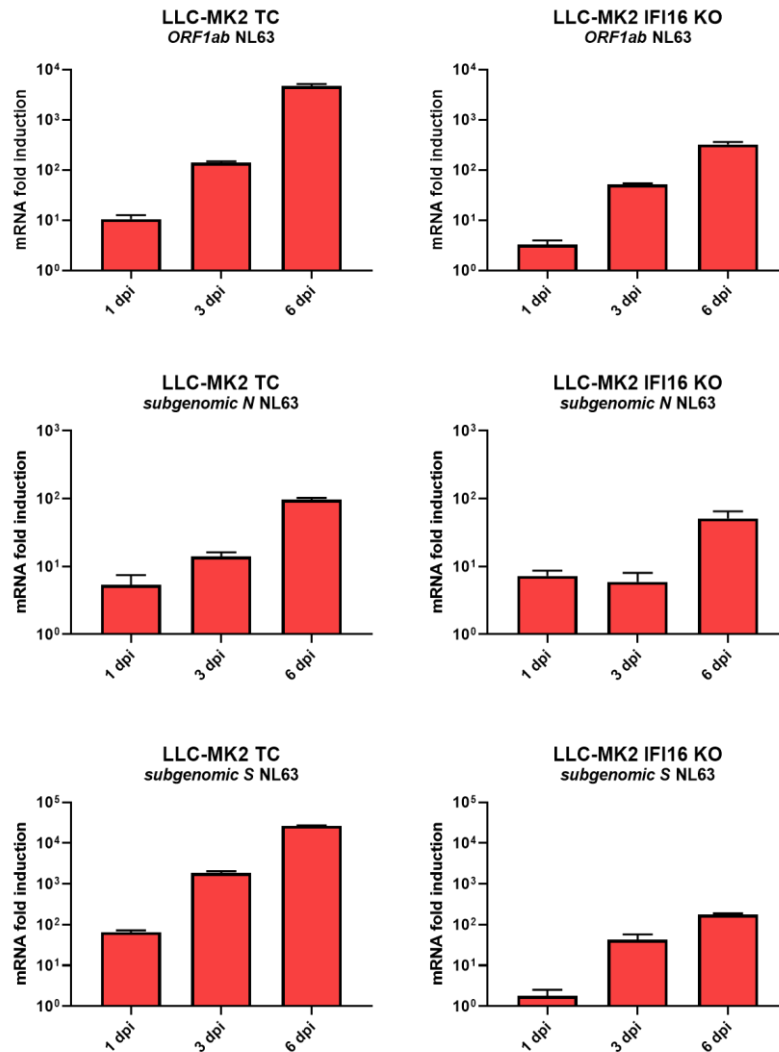
Figure 18. <u>Viral gene transcription upon NL63 infection in LLC-MK2 TC and LLC-MK2 IFI16 KO cells</u>. LLC-MK2 TC and LLC-MK2 IFI16 KO cells were infected with NL63 MOI 1 and at the indicated time points, total RNA was isolated from cells and virus RNA levels were determined by means of RT-qPCR, with ORF1ab specific primers detecting only the viral RNA genome and with primers detecting only subgenomic N and S mRNAs. Graphs show the average fold change and SD for each time-point compared to the 2 h time-point. Intracellular viral RNA levels were corrected for total cell numbers using GAPDH as a standard.

To complete the characterization of NL63 infection in the absence of IFI16, we wanted to determine whether LLC-MK2 IFI16 KO cells could induce an immune response upon NL63 infection. To this aim, we checked the RNA levels of the antiviral cytokine IFNβ, as key factor involved in the antiviral response to coronaviruses, and of the ISGs Mx1 and IFIT1, in both TC and IFI16 KO LLC-MK2 cells infected by NL63 at MOI 1. Compared to LLC-MK2 TC cells, where the innate immunity markers are almost not detectable, in LLC-MK2 IFI16 KO cells there is a substantial stimulation of the innate immune response, starting from 1 dpi (Figure 19).
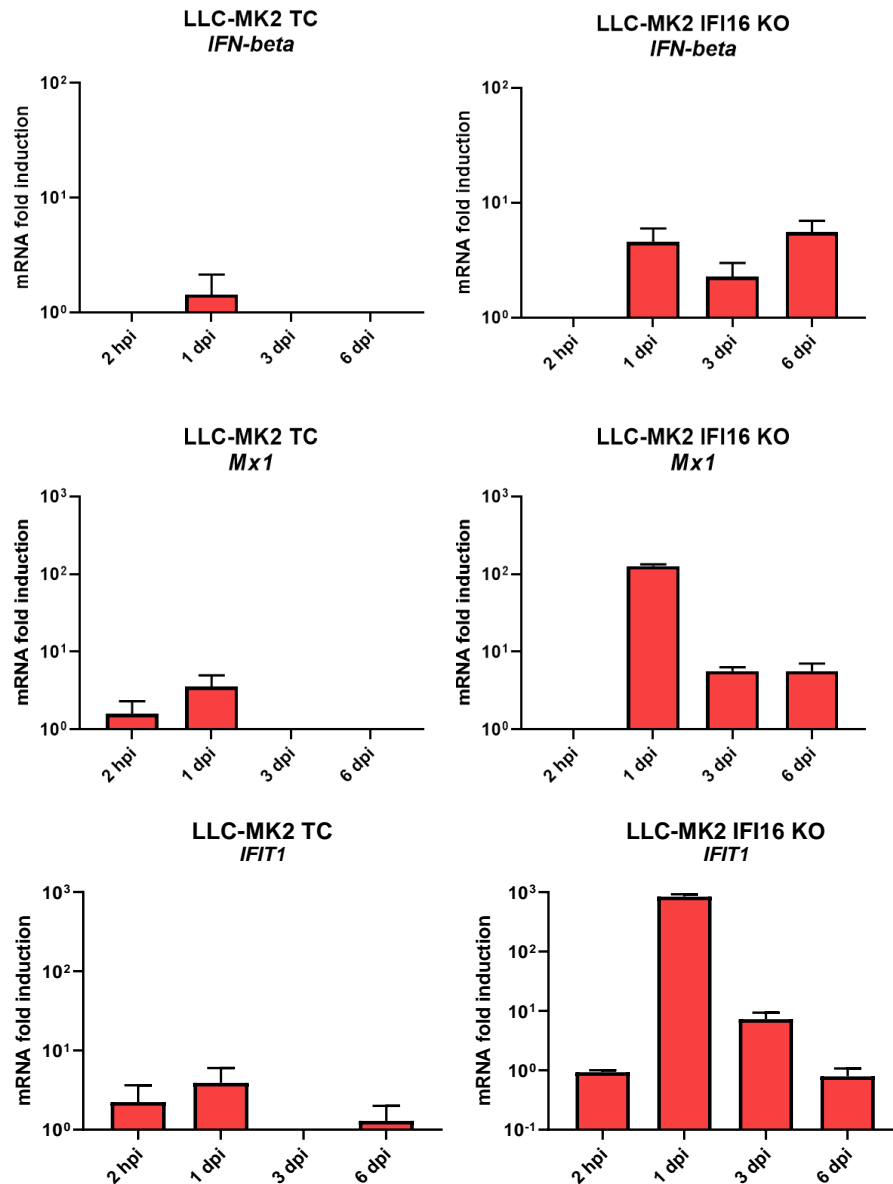
Figure 19. Innate immune transcripts in LLC-MK2 TC and LLC-MK2 IFI16 KO cells upon NL63 infection. LLC-MK2 TC and LLC-MK2 IFI16 KO cells were infected with NL63 MOI 1 and at the indicated time points, total RNA was isolated from cells and virus RNA levels were determined by means of RT-qPCR, with IFNβ and Mx1 specific primers. Graphs show the average fold change and SD for each time-point. Values were normalized to the housekeeping GAPDH gene mRNA and plotted as fold induction relative to mock-infected cells.

Finally, we analyzed the protein expression of NL63 nucleoprotein in LLC-MK2 TC and LLC-MK2 IFI16 KO cells infected by NL63 at MOI 1. The expression levels of NP are very much decreased in absence of IFI16, and this is consistent with the lowering of genomic and subgenomic RNA levels in LLC-MK2 IFI16 KO. The western blot analysis of IFI16 expression confirms that NL63 infection does not modulate the levels of the innate immune sensor (Figure 20).
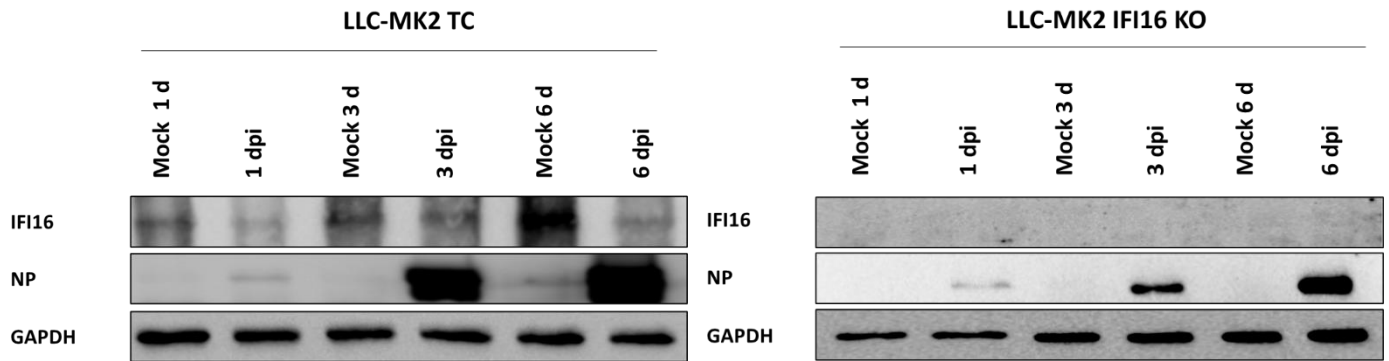

Figure 20. <u>NP and IFI16 expression in LLC-MK2 TC and LLC-MK2 IFI16 KO</u>. Cellular extracts from LLC-MK2 TC and LLC-MK2 IFI16 KO cells infected with NL63 at MOI 1 were collected at 1 dpi, 3 dpi and 6 dpi to evaluate NP and IFI16 expression. The housekeeping gene GAPDH was used as loading control for protein normalization.

5. DISCUSSION

The immune system of bats has evolved over time to limit excessive inflammation derived from the high metabolic demand of flight. These alterations have induced a state of tolerance against viral infections, making bats ideal reservoir hosts for many viruses, including SARS-like coronaviruses (SARS-CoV, MERS-CoV, SARS-CoV2-2) (Luis *et al.*, 2013; Zhang *et al.*, 2012). In this regard, recent genomic analysis revealed the loss of the entire PYHIN gene family in bats; members of this family are important immune sensors of intracellular self and foreign DNA, as well as activators of the inflammasome and/or interferon pathways (Ahn *et al.*, 2016). Among them, IFI16 is a cellular host restriction factor that has been well characterized as a nuclear DNA sensor (Unterholzner *et al.*, 2011), capable of binding to incoming viral DNA at the nuclear periphery (Howard and Cristea, 2020). Evidence demonstrates that upon binding to viral DNA, IFI16 undergoes oligomerization and recruits other host factors, necessary to build antiviral support to activate immune signaling and suppress transcription (Howard and Cristea, 2020). In addition, several studies have attributed to IFI16 the capacity to limit infection of some RNA viruses, including IAV (Jiang *et al.*, 2021), CHIKV (Kim *et al.*, 2020) and the replication of PPRSV-2 (Chang *et al.*, 2019).

According to this background, we used the low-pathogenic HCoV-NL63, to investigate the role of IFI16 during coronavirus infection in the monkey kidney-derived epithelial cell line LLC-MK2.

Firstly, we defined the kinetic of NL63 in our cellular model; thus, the RNA levels of ORF1ab in NL63-LLC-MK2-infected cells suggest that the virus starts to replicate at 1 dpi, reaching a peak of replication at 4 dpi. Similarly, the transcription of NL63 starts to be detectable at 1 dpi, to peak at 4 dpi, as demonstrated by the sgRNA levels. These results are supported by the plaque assay, performed on supernatants of LLC-MK2 cells infected with NL63 at MOI 1, showing a viral titer of 4×10^3 PFU/ml at 5 dpi. Then, to confirm the success of infection, through a western blot analysis we demonstrated that the NP protein levels increase over time, peaking at 4 dpi, while are absent in the non-infected cells. Also, we investigated the expression of IFI16, showing that NL63 infection does not modulate the levels of IFI16. All together these results confirmed the ability of NL63 to infect LLC-MK2. Even though there are evidence showing that LLC-MK2 retain a functional IFN system, produce IFNs response to virus infection, and exhibit an antiviral state (Nao *et al.*, 2019), we demonstrated that LLC-MK2 cells do not mount any IFN response to NL63 infection. Indeed, the real-time qPCR analysis revealed that upon NL63 infection, there is no induction of *IFN-β* and *IFN-λ1* and accordingly

mRNA levels of the ISGs *Mx1* and *Mx2* were not affected. Thus, the observed dampened immune response could be a viral escape mechanism, a possible explanation for the active replication of NL63 in these cells.

Given that HCoVs replicate in the cytoplasm (Roingeard *et al.*, 2022) and that IFI16 can bind to RNA viral genomes (Jiang *et al.*, 2021; Kim *et al.*, 2020), we asked whether IFI16 could form a complex with NP. Firstly, through immunofluorescence analysis we demonstrated the cytoplasmatic re-localization of IFI16 upon NL63 infection; indeed, in infected cells, IFI16 co-localizes with the viral NP protein. The coimmunoprecipitation assay confirms that IFI16 interacts with the RNA-binding protein NP. Further studies are being performed to gain more insight into this interaction and understand whether it depends on the binding of IFI16 to the viral RNA genome. Whether this interaction may affect the HCoV viral genome sensing, the antiviral response, or its replication remains to be established.

The experiments performed on LLC-MK2 TC and LLC-MK2 IFI16 KO cells suggest that in absence of IFI16, NL63 replicates less and reduces the transcription of viral genes, in accordance with an increase of innate immunity. Also, the expression levels of the viral nucleoprotein NP are very much reduced in absence of IFI16. The ability of IFI16 to translocate to the cytoplasm following various stimuli has already been described in the literature (Costa *et al.*, 2011; Dell'Oste *et al.*, 2014), yet IFI16 activity has always been linked to the inhibition of viral infection rather than promotion. Recent evidence demonstrated the capacity of IFI16 to bind viral RNA (Jiang *et al.*, 2021; Kim *et al.*, 2020).

It is likely that IFI16 binds NL63 RNA, hiding it from other innate immune sensors, allowing the virus to escape from innate immunity activation. Thus, in absence of IFI16 the viral RNA can be recognized by innate immune sensors, such as RIG-I and MDA5, activating the innate immune response that contrasts the replication and transcription of viral genes. To test this hypothesis, further studies will be made to demonstrate whether IFI16 could interact with the viral RNA of NL63 by the means of different assays, such as Surface Plasmon Resonance (SPR) and RNA-immunoprecipitation (RIP).

Overall, this study will contribute to filling the gap in knowledge about the role of the innate sensor IFI16 in controlling HCoV replication. Characterizing the molecular machinery involved in host-virus interaction and inflammation control is crucial for identifying druggable targets. The long-range goal of this project is to deepen our understanding of the role of IFI16 in triggering abnormal inflammatory reactions in HCoV-infected human epithelial cells. This

understanding will help develop novel therapeutic approaches not only for HCoV-related diseases but also for other RNA virus diseases.

6. BIBLIOGRAPHY

Adil MT, Rahman R, Whitelaw D, Jain V, Al-Taan O, Rashid F, Munasinghe A, Jambulingam P. SARS-CoV-2 and the pandemic of COVID-19. Postgrad Med J. 2021 Feb;97(1144):110-116. doi: 10.1136/postgradmedj-2020-138386. Epub 2020 Aug 11. PMID: 32788312

Ahn, M., Cui, J., Irving, A. T., & Lin-FaWang. (2016). Unique Loss of the PYHIN Gene Family in Bats Amongst Mammals: Implications for Inflammasome Sensing. *Nature*, 1-7.

Artika IM, Dewantari AK, Wiyatno A. Molecular biology of coronaviruses: current knowledge. Heliyon. 2020 Aug;6(8): e04743. doi: 10.1016/j.heliyo. 2020.e04743. Epub 2020 Aug 17. PMID: 32835122; PMCID: PMC7430346

Banerjee A, Kulcsar K, Misra V, Frieman M, Mossman K. Bats and Coronaviruses. Viruses. 2019 Jan 9;11(1):41. doi: 10.3390/v11010041. PMID: 30634396; PMCID: PMC6356540

Bawadekar, Marco De Andrea, Irene Lo Cigno, Gianluca Baldanzi, Valeria Caneparo, Andrea Graziani, Santo Landolfo, Marisa Gariglio ,The Extracellular IFI16 Protein Propagates Inflammation in Endothelial Cells Via p38 MAPK and NF-κB p65 Activation, published 1 jun 2015

Berry M, Gamieldien J, Fielding BC. Identification of new respiratory viruses in the new millennium. Viruses. 2015 Mar 6;7(3):996-1019. doi: 10.3390/v7030996. PMID: 25757061; PMCID: PMC4379558

Bosso M, Kirchhoff F. Emerging Role of PYHIN Proteins as Antiviral Restriction Factors. Viruses. 2020 Dec 18;12(12):1464. doi: 10.3390/v12121464. PMID: 33353088; PMCID: PMC7767131.

Bosso, M., Bozzo, C. P., Hotter, D., Volcic, M., Stürzel, C. M., Rammelt, A., . . . Sau, D. (2020). Nuclear PYHIN proteins target the host transcription factor Sp1 thereby restricting HIV-1 in human macrophages and CD4+ T cells. *Plos Pathogens*, 1-30.

Canton J, Fehr AR, Fernandez-Delgado R, Gutierrez-Alvarez FJ, Sanchez-Aparicio MT, García-Sastre A, Perlman S, Enjuanes L, Sola I. MERS-CoV 4b protein interferes with the NF-κB-dependent innate immune response during infection. PLoS Pathog. 2018 Jan 25;14(1): e1006838. doi: 10.1371/journal.ppat.1006838. PMID: 29370303; PMCID: PMC5800688

Chang, Xiaobo, Xibao Shi, Xiaozhuan Zhang, Li Wang, Xuewu Li, Aiping Wang, Ruiguang Deng, Enmin Zhou, and Gaiping Zhang. 2019. "IFI16 Inhibits Porcine Reproductive and Respiratory Syndrome Virus 2 Replication in a MAVS-Dependent Manner in MARC-145 Cells" *Viruses* 11, no. 12: 1160.

Chen B, Tian EK, He B, Tian L, Han R, Wang S, Xiang Q, Zhang S, El Arnaout T, Cheng W. Overview of lethal human coronaviruses. Signal Transduct Target Ther. 2020 Jun 10;5(1):89. doi: 10.1038/s41392-020-0190-2. PMID: 32533062; PMCID: PMC7289715

Connolly DJ, Bowie AG. The emerging role of human PYHIN proteins in innate immunity: implications for health and disease. Biochem Pharmacol. 2014 Dec 1;92(3):405-14. doi: 10.1016/j.bcp.2014.08.031. Epub 2014 Sep 6. PMID: 25199457.

Costa S, Borgogna C, Mondini M, De Andrea M, Meroni PL, Berti E, Gariglio M, Landolfo S. Redistribution of the nuclear protein IFI16 into the cytoplasm of ultraviolet B-exposed keratinocytes as a mechanism of autoantigen processing. Br J Dermatol. 2011 Feb;164(2):282-90. doi: 10.1111/j.1365-2133.2010.10097.x. PMID: 20973769.

Cridland JA, Curley EZ, Wykes MN, Schroder K, Sweet MJ, Roberts TL, Ragan MA, Kassahn KS, Stacey KJ. The mammalian PYHIN gene family: phylogeny, evolution and expression. BMC Evol Biol. 2012 Aug 7;12:140. doi: 10.1186/1471-2148-12-140. PMID: 22871040; PMCID: PMC3458909.

Crouse J, Kalinke U, Oxenius A. Regulation of antiviral T cell responses by type I interferons. Nat Rev Immunol. 2015 Apr;15(4):231-42. doi: 10.1038/nri3806. Epub 2015 Mar 20. PMID: 25790790.

Cui J, Li F, Shi ZL. Origin and evolution of pathogenic coronaviruses. Nat Rev Microbiol. 2019 Mar;17(3):181-192. doi: 10.1038/s41579-018-0118-9. PMID: 30531947; PMCID: PMC7097006

Deng X, Baker SC. Coronaviruses: Molecular Biology (*Coronaviridae*). Encyclopedia of Virology. 2021:198–207. doi: 10.1016/B978-0-12-814515-9.02550-9. Epub 2021 Mar 1. PMCID: PMC7917440

Denney L, Ho LP. The role of respiratory epithelium in host defence against influenza virus infection. Biomed J. 2018 Aug;41(4):218-233. doi: 10.1016/j.bj.2018.08.004. Epub 2018 Sep 10. PMID: 30348265; PMCID: PMC6197993.

Dell'Oste V, Gatti D, Gugliesi F, De Andrea M, Bawadekar M, Lo Cigno I, Biolatti M, Vallino M, Marschall M, Gariglio M, Landolfo S. Innate nuclear sensor IFI16 translocates into the cytoplasm during the early stage of in vitro human cytomegalovirus infection and is entrapped in the egressing virions during the late stage. J Virol. 2014 Jun;88(12):6970-82. doi: 10.1128/JVI.00384-14. Epub 2014 Apr 2. PMID: 24696486; PMCID: PMC4054358.

Fehr AR, Perlman S. Coronaviruses: an overview of their replication and pathogenesis. Methods Mol Biol. 2015; 1282:1-23. doi: 10.1007/978-1-4939-2438-7_1. PMID: 25720466; PMCID: PMC4369385

Forni D, Cagliani R, Clerici M, Sironi M. Molecular Evolution of Human Coronavirus Genomes. Trends Microbiol. 2017 Jan;25(1):35-48. doi: 10.1016/j.tim.2016.09.001. Epub 2016 Oct 19. PMID: 27743750; PMCID: PMC7111218

Hartenian E, Nandakumar D, Lari A, Ly M, Tucker JM, Glaunsinger BA. The molecular virology of coronaviruses. J Biol Chem. 2020 Sep 11;295(37):12910-12934. doi: 10.1074/jbc. REV120.013930. Epub 2020 Jul 13. PMID: 32661197; PMCID: PMC7489918

Hamre D, Procknow JJ. A new virus isolated from the human respiratory tract. Proc Soc Exp Biol Med. 1966 Jan;121(1):190-3. doi: 10.3181/00379727-121-30734. PMID: 4285768

Herzog, P., Drosten, C., & Müller, M. A. (2008). Plaque assay for human coronavirus NL63 using human colon carcinoma cells. *Virology Journal*, 1-9.

Hoffmann M, Kleine-Weber H, Pöhlmann S. A Multibasic Cleavage Site in the Spike Protein of SARS-CoV-2 Is Essential for Infection of Human Lung Cells. Mol Cell. 2020 May 21;78(4):779-784.e5. doi: 10.1016/j.molcel.2020.04.022. Epub 2020 May 1. PMID: 32362314; PMCID: PMC7194065

Howard, T. R., & Cristea, I. M. (2020). Interrogating host antiviral environments driven by nuclear DNA sensing: A multi-omic perspective. Biomolecules, 1591

Hu Y, Liu L, Lu X. Regulation of Angiotensin-Converting Enzyme 2: A Potential Target to Prevent COVID-19? Front Endocrinol (Lausanne). 2021 Oct 22;12:725967. doi: 10.3389/fendo.2021.725967. PMID: 34745001; PMCID: PMC8569797

Irving, A. T., Ahn, M., Goh, G., & Anderson, D. E. (2021). Lessons from the host defences of bats, a unique viral reservoir. *Nature*, 363-370.

Islam A, Ferdous J, Islam S, Sayeed MA, Dutta Choudhury S, Saha O, Hassan MM, Shirin T. Evolutionary Dynamics and Epidemiology of Endemic and Emerging Coronaviruses in Humans, Domestic Animals, and Wildlife. Viruses. 2021 Sep 23;13(10):1908. doi: 10.3390/v13101908. PMID: 34696338; PMCID: PMC8537103

Janeway CA Jr, Travers P, Walport M, et al. Immunobiology: The Immune System in Health and Disease. 5th edition. New York: Garland Science; 2001. Principles of innate and adaptive immunity. Available from: https://www.ncbi.nlm.nih.gov/books/NBK27090/

Jin T, Perry A, Jiang J, Smith P, Curry JA, Unterholzner L, Jiang Z, Horvath G, Rathinam VA, Johnstone RW, Hornung V, Latz E, Bowie AG, Fitzgerald KA, Xiao TS. Structures of the HIN domain:DNA complexes reveal ligand binding and activation mechanisms of the AIM2 inflammasome and IFI16 receptor. Immunity. 2012 Apr 20;36(4):561-71. doi: 10.1016/j.immuni.2012.02.014. Epub 2012 Apr 5. PMID: 22483801; PMCID: PMC3334467.

Jiang Z, Wei F, Zhang Y, Wang T, Gao W, Yu S, Sun H, Pu J, Sun Y, Wang M, Tong Q, Gao C, Chang KC, Liu J. IFI16 directly senses viral RNA and enhances RIG-I transcription and activation to restrict influenza virus infection. Nat Microbiol. 2021 Jul;6(7):932-945. doi: 10.1038/s41564-021-00907-x. Epub 2021 May 13. PMID: 33986530.

Kase Y, Okano H. Neurological pathogenesis of SARS-CoV-2 (COVID-19): from virological features to clinical symptoms. Inflamm Regen. 2021 May 7;41(1):15. doi: 10.1186/s41232-021-00165-8. PMID: 33962695; PMCID: PMC8103065

Kasuga, Y., Zhu, B., Jang, KJ. *et al.* Innate immune sensing of coronavirus and viral evasion strategies. *Exp Mol Med* **53**, 723–736 (2021). https://doi.org/10.1038/s12276-021-00602-1;published 06 may 2021

Kim B, Arcos S, Rothamel K, Jian J, Rose KL, McDonald WH, Bian Y, Reasoner S, Barrows NJ, Bradrick S, Garcia-Blanco MA, Ascano M. Discovery of Widespread Host Protein Interactions with the Pre-replicated Genome of CHIKV Using VIR-CLASP. Mol Cell. 2020 May 21;78(4):624-640.e7. doi: 10.1016/j.molcel.2020.04.013. Epub 2020 May 6. PMID: 32380061; PMCID: PMC7263428.

Kuba K, Imai Y, Rao S, Gao H, Guo F, Guan B, Huan Y, Yang P, Zhang Y, Deng W, Bao L, Zhang B, Liu G, Wang Z, Chappell M, Liu Y, Zheng D, Leibbrandt A, Wada T, Slutsky AS, Liu D, Qin C, Jiang C, Penninger JM. A crucial role of angiotensin converting enzyme 2 (ACE2) in SARS coronavirus-induced lung injury. Nat Med. 2005 Aug;11(8):875-9. doi: 10.1038/nm1267. Epub 2005 Jul 10. PMID: 16007097; PMCID: PMC7095783

Kumar H, Kawai T, Akira S. Pathogen recognition by the innate immune system. Int Rev Immunol. 2011 Feb;30(1):16-34. doi: 10.3109/08830185.2010.529976. PMID: 21235323.

Kumar A, Ishida R, Strilets T, Cole J, Lopez-Orozco J, Fayad N, Felix-Lopez A, Elaish M, Evseev D, Magor KE, Mahal LK, Nagata LP, Evans DH, Hobman TC. SARS-CoV-2 Nonstructural Protein 1 Inhibits the Interferon Response by Causing Depletion of Key Host Signaling Factors. J Virol. 2021 Jun 10;95(13):e0026621. doi: 10.1128/JVI.00266-21. Epub 2021 Jun 10. PMID: 34110264; PMCID: PMC8316110.

Loo YM, Gale M Jr. Immune signaling by RIG-I-like receptors. Immunity. 2011 May 27;34(5):680-92. doi: 10.1016/j.immuni.2011.05.003. PMID: 21616437; PMCID: PMC3177755.

Li W, Sui J, Huang IC, Kuhn JH, Radoshitzky SR, Marasco WA, Choe H, Farzan M. The S proteins of human coronavirus NL63 and severe acute respiratory syndrome coronavirus bind overlapping regions of ACE2. Virology. 2007 Oct 25;367(2):367-74. doi: 10.1016/j.virol.2007.04.035. Epub 2007 Jul 12. PMID: 17631932; PMCID: PMC2693060

Li X, Luk HKH, Lau SKP, Woo PCY. Human Coronaviruses: General Features. Reference Module in Biomedical Sciences. 2019: B978-0-12-801238-3.95704-0. doi: 10.1016/B978-0-12-801238-3.95704-0. Epub 2019 Mar 11. PMCID: PMC7157439

Li JY, Zhou ZJ, Wang Q, He QN, Zhao MY, Qiu Y, Ge XY. Innate Immunity Evasion Strategies of Highly Pathogenic Coronaviruses: SARS-CoV, MERS-CoV, and SARS-CoV-2. Front Microbiol. 2021 Oct 29;12:770656. doi: 10.3389/fmicb.2021.770656. PMID: 34777324; PMCID: PMC8586461.

Liu Q, Chi S, Dmytruk K, Dmytruk O, Tan S. Coronaviral Infection and Interferon Response: The Virus-Host Arms Race and COVID-19. Viruses. 2022 Jun 21;14(7):1349. doi: 10.3390/v14071349. PMID: 35891331; PMCID: PMC9325157.

Ludlow LE, Johnstone RW, Clarke CJ. The HIN-200 family: more than interferon-inducible genes? Exp Cell Res. 2005 Aug 1;308(1):1-17. doi: 10.1016/j.yexcr.2005.03.032. PMID: 15896773.

Luis AD, Hayman DT, O'Shea TJ, Cryan PM, Gilbert AT, Pulliam JR, Mills JN, Timonin ME, Willis CK, Cunningham AA, Fooks AR, Rupprecht CE, Wood JL, Webb CT. A comparison of bats and rodents as reservoirs of zoonotic viruses: are bats special? Proc Biol Sci. 2013 Feb 1;280(1756):20122753. doi: 10.1098/rspb.2012.2753. PMID: 23378666; PMCID: PMC3574368.

Masters, P. S., & Perlman, S. (2013). Chapter 28 Coronaviridae (Vol. 1). (D. Knipe, & P. M. Howley, Eds.) Philadelphia: Lippincott Williams and Wilkins

Mathewson AC, Bishop A, Yao Y, Kemp F, Ren J, Chen H, Xu X, Berkhout B, van der Hoek L, Jones IM. Interaction of severe acute respiratory syndrome-coronavirus and NL63 coronavirus spike proteins with angiotensin converting enzyme-2. J Gen Virol. 2008 Nov;89(Pt 11):2741-2745. doi: 10.1099/vir.0.2008/003962-0. PMID: 18931070; PMCID: PMC2886958

Masters PS. The molecular biology of coronaviruses. Adv Virus Res. 2006;66: 193-292. doi: 10.1016/S0065-3527(06)66005-3. PMID: 16877062; PMCID: PMC7112330

Merkl, P. E., Orzalli, M. H., & Knipe, D. M. (2018). Mechanism of host IFI16, PML, and Daxx protein restriction of Herpes Simplex Virus 1 replication. Journal of Virology, e00057-18

McIntosh K, Dees JH, Becker WB, Kapikian AZ, Chanock RM. Recovery in tracheal organ cultures of novel viruses from patients with respiratory disease. Proc Natl Acad Sci U S A. 1967 Apr;57(4):933-40. doi: 10.1073/pnas.57.4.933. PMID: 5231356; PMCID: PMC224637

Miyanaga A, Fushinobu S, Ito K, Wakagi T. Crystal structure of cobalt-containing nitrile hydratase. Biochem Biophys Res Commun. 2001 Nov 16;288(5):1169-74. doi: 10.1006/bbrc.2001.5897. PMID: 11700034.

Milewska A, Nowak P, Owczarek K, Szczepanski A, Zarebski M, Hoang A, Berniak K, Wojarski J, Zeglen S, Baster Z, Rajfur Z, Pyrc K. Entry of Human Coronavirus NL63 into the Cell. J Virol. 2018 Jan 17;92(3):e01933-17. doi: 10.1128/JVI.01933-17. PMID: 29142129; PMCID: PMC5774871

Minakshi, R., Padhan, K., Rani, M., Khan, N., Ahmad, F., & Jameel, S. (2009). The SARS Coronavirus 3a Protein Causes Endoplasmic Reticulum Stress and Induces Ligand-Independent Downregulation of the Type 1 Interferon Receptor. *Plos One*, 1-10.

Millet JK, Jaimes JA, Whittaker GR. Molecular diversity of coronavirus host cell entry receptors. FEMS Microbiol Rev. 2021 May 5;45(3): fuaa057. doi: 10.1093/femsre/fuaa057. PMID: 33118022; PMCID: PMC7665467

Mishra S, Raj AS, Kumar A, Rajeevan A, Kumari P, Kumar H. Innate immune sensing of influenza A viral RNA through IFI16 promotes pyroptotic cell death. iScience. 2021 Dec 31;25(1):103714. doi: 10.1016/j.isci.2021.103714. PMID: 35072006; PMCID: PMC8762390.

Mulabbi EN, Tweyongyere R, Byarugaba DK. The history of the emergence and transmission of human coronaviruses. Onderstepoort J Vet Res. 2021 Feb 10;88(1): e1-e8. doi: 10.4102/ojvr. V 88i1.1872. PMID: 33567843; PMCID: PMC7876959

Nao, N., Sato, K., Yamagishi, J., Tahara, M., Nakatsu, Y., Seki, F., . . . Takeda, M. (2019). Consensus and variations in cell line specificity among human metapneumovirus strains. PLoS One, 1-21

Parisi, O. I., Dattilo, M., Patitucci, F., Malivindi, R., Delbue, S., Ferrante, P., . . . Selmin, F. (2021). Design and development of plastic antibodies against SARS-CoV-2 RBD based on molecularly imprinted polymers that inhibit in vitro virus infection. *Nanoscale*, 16821-17184.

Pyrc K, Jebbink MF, Berkhout B, van der Hoek L. Genome structure and transcriptional regulation of human coronavirus NL63. Virol J. 2004 Nov 17;1:7. doi: 10.1186/1743-422X-1-7. PMID: 15548333; PMCID: PMC538260

Pyrc K, Berkhout B, van der Hoek L. The novel human coronaviruses NL63 and HKU1. J Virol. 2007 Apr;81(7):3051-7. doi: 10.1128/JVI.01466-06. Epub 2006 Nov 1. PMID: 17079323; PMCID: PMC1866027

Prompetchara, E., Ketloy, C., & Palaga, T. (2020). Immune responses in COVID-19 and potential vaccines: Lessons learned from SARS and MERS epidemic. *Allergy and Immunology*.

Rahman MT, Sobur MA, Islam MS, Ievy S, Hossain MJ, El Zowalaty ME, Rahman AT, Ashour HM. Zoonotic Diseases: Etiology, Impact, and Control. Microorganisms. 2020 Sep 12;8(9):1405. doi: 10.3390/microorganisms8091405. PMID: 32932606; PMCID: PMC7563794

Rajapakse N, Dixit D. Human and novel coronavirus infections in children: a review. Paediatr Int Child Health. 2021 Feb;41(1):36-55. doi: 10.1080/20469047.2020.1781356. Epub 2020 Jun 25. PMID: 32584199

Rinki Minakshi,Kartika Padhan,Manjusha Rani,Nabab Khan,Faizan Ahmed,Shahid Jameel. The SARS Coronavirus 3a Protein Causes Endoplasmic Reticulum Stress and Induces Ligand-Independent Downregulation of the Type 1 Interferon Receptor; Published: December 17, 2009.

Ruiz-Aravena M, McKee C, Gamble A, Lunn T, Morris A, Snedden CE, Yinda CK, Port JR, Buchholz DW, Yeo YY, Faust C, Jax E, Dee L, Jones DN, Kessler MK, Falvo C, Crowley D, Bharti N, Brook CE, Aguilar HC, Peel AJ, Restif O, Schountz T, Parrish CR, Gurley ES, Lloyd-Smith JO, Hudson PJ, Munster VJ, Plowright RK. Ecology, evolution and spillover of coronaviruses from bats. Nat Rev Microbiol. 2022 May;20(5):299-314. doi: 10.1038/s41579-021-00652-2. Epub 2021 Nov 19. Erratum in: Nat Rev Microbiol. 2022 Jan 13: PMID: 34799704; PMCID: PMC8603903

Saeid Najafi Fard, Linda Petrone, Elisa Petruccioli, Tonino Alonzi, Giulia Matusali, Francesca Colavita, Concetta Castilletti, Maria Rosaria Capobianchi, Delia Goletti. In Vitro Models for Studying Entry, Tissue Tropism, and Therapeutic Approaches of Highly Pathogenic Coronaviruses.doi:101155/2021/8856018; pubmed id:34239932; pub.1139080728

Sawicki SG, Sawicki DL, Siddell SG. A contemporary view of coronavirus transcription. J Virol. 2007 Jan;81(1):20-9. doi: 10.1128/JVI.01358-06. Epub 2006 Aug 23. PMID: 16928755; PMCID: PMC1797243

Schneider WM, Chevillotte MD, Rice CM. Interferon-stimulated genes: a complex web of host defenses. Annu Rev Immunol. 2014;32:513-45. doi: 10.1146/annurev-immunol-032713-120231. Epub 2014 Feb 6. PMID: 24555472; PMCID: PMC4313732.

Schattgen SA, Fitzgerald KA. The PYHIN protein family as mediators of host defenses. Immunol Rev. 2011 Sep;243(1):109-18. doi: 10.1111/j.1600-065X.2011.01053.x. PMID: 21884171.

Seth RB, Sun L, Ea CK, Chen ZJ. Identification and characterization of MAVS, a mitochondrial antiviral signaling protein that activates NF-kappaB and IRF 3. Cell. 2005 Sep 9;122(5):669-82. doi: 10.1016/j.cell.2005.08.012. PMID: 16125763.

Shaw N, Liu ZJ. Role of the HIN domain in regulation of innate immune responses. Mol Cell Biol. 2014 Jan;34(1):2-15. doi: 10.1128/MCB.00857-13. Epub 2013 Oct 28. PMID: 24164899; PMCID: PMC3911281.

 Streicher F, Jouvenet N. Stimulation of Innate Immunity by Host and Viral RNAs. Trends Immunol. 2019 Dec;40(12):1134-1148. doi: 10.1016/j.it.2019.10.009. Epub 2019 Nov 14. PMID: 31735513.

Stehlik C. The PYRIN domain in signal transduction. Curr Protein Pept Sci. 2007 Jun;8(3):293-310. doi: 10.2174/138920307780831857. PMID: 17584123; PMCID: PMC4259900.

Sun L, Xing Y, Chen X, Zheng Y, Yang Y, Nichols DB, Clementz MA, Banach BS, Li K, Baker SC, Chen Z. Coronavirus papain-like proteases negatively regulate antiviral innate immune response through disruption of STING-mediated signaling. PLoS One. 2012;7(2):e30802. doi: 10.1371/journal.pone.0030802. Epub 2012 Feb 1. PMID: 22312431; PMCID: PMC3270028.

Turvey SE, Broide DH. Innate immunity. J Allergy Clin Immunol. 2010 Feb;125(2 Suppl 2): S24-32. doi: 10.1016/j.jaci.2009.07.016. Epub 2009 Nov 24. PMID: 19932920; PMCID: PMC2832725

Unterholzner, L., Keating, S. E., Baran, M., Horan, K. A., Jensen, S. B., Sharma, S., . . . Bowie, A. G. (2011). IFI16 is an innate immune sensor for intracellular DNA. *Nature Immunology*, 1-19.

van der Hoek L, Pyrc K, Berkhout B. Human coronavirus NL63, a new respiratory virus. FEMS Microbiol Rev. 2006 Sep;30(5):760-73. doi: 10.1111/j.1574-6976.2006.00032. x . PMID: 16911043; PMCID: PMC7109777

van der Hoek L, Pyrc K, Jebbink MF, Vermeulen-Oost W, Berkhout RJ, Wolthers KC, Wertheim-van Dillen PM, Kaandorp J, Spaargaren J, Berkhout B. Identification of a new human coronavirus. Nat Med. 2004 Apr;10(4):368-73. doi: 10.1038/nm1024. Epub 2004 Mar 21. PMID: 15034574; PMCID: PMC7095789

V'kovski P, Kratzel A, Steiner S, Stalder H, Thiel V. Coronavirus biology and replication: implications for SARS-CoV-2. Nat Rev Microbiol. 2021 Mar;19(3):155-170. doi: 10.1038/s41579-020-00468-6. Epub 2020 Oct 28. PMID: 33116300; PMCID: PMC7592455

Woo PC, Lau SK, Chu CM, Chan KH, Tsoi HW, Huang Y, Wong BH, Poon RW, Cai JJ, Luk WK, Poon LL, Wong SS, Guan Y, Peiris JS, Yuen KY. Characterization and complete genome sequence of a novel coronavirus, coronavirus HKU1, from patients with pneumonia. J Virol. 2005 Jan;79(2):884-95. doi: 10.1128/JVI.79.2.884-895.2005. PMID: 15613317; PMCID: PMC538593

Woo J, Lee EY, Lee M, Kim T, Cho YE. An in vivo cell-based assay for investigating the specific interaction between the SARS-CoV N-protein and its viral RNA packaging sequence. Biochem Biophys Res Commun. 2019 Dec 10;520(3):499-506. doi: 10.1016/j.bbrc.2019.09.115. Epub 2019 Oct 5. PMID: 31594639; PMCID: PMC7092827

Xia H, Cao Z, Xie X, Zhang X, Chen JY, Wang H, Menachery VD, Rajsbaum R, Shi PY. Evasion of Type I Interferon by SARS-CoV-2. Cell Rep. 2020 Oct 6;33(1):108234. doi: 10.1016/j.celrep.2020.108234. Epub 2020 Sep 19. PMID: 32979938; PMCID: PMC7501843.

Xie J, Li Y, Shen X, Goh G, Zhu Y, Cui J, Wang LF, Shi ZL, Zhou P. Dampened STING-Dependent Interferon Activation in Bats. Cell Host Microbe. 2018 Mar 14;23(3):297-301.e4. doi: 10.1016/j.chom.2018.01.006. Epub 2018 Feb 22. PMID: 29478775; PMCID: PMC7104992.

Yang, L., Xie, X., Tu, Z. *et al.* The signal pathways and treatment of cytokine storm in COVID-19. *Sig Transduct Target Ther* 6, 255 (2021). https://doi.org/10.1038/s41392-021-00679-0

Ye ZW, Yuan S, Yuen KS, Fung SY, Chan CP, Jin DY. Zoonotic origins of human coronaviruses. Int J Biol Sci. 2020 Mar 15;16(10):1686-1697. doi: 10.7150/ijbs.45472. PMID: 32226286; PMCID: PMC7098031

Yoriyuki Konno, Izumi Kimur, Keiya Uriui, Masaya Fukushi, Takashi Irie, Yoshio Koyanagi, Daniel Sauter, Robert J. Gifford, USFQ-COVID19 Consortium, So Nakagawa, Kei Sato. SARS-CoV-2 ORF3b Is a Potent Interferon Antagonist Whose Activity Is Increased by a Naturally Occurring Elongation Variant;published:September 2020.

Zhang, G., Cowled, C., Shi, Z., Huang, Z., Bishop-Lilly, K. A., Fang, X., . . . Jiang, X. (2012). Comparative Analysis of Bat Genomes Provides Insight into the Evolution of Flight and Immunity. *Science* , 456-460.

Zhu N, Zhang D, Wang W, Li X, Yang B, Song J, Zhao X, Huang B, Shi W, Lu R, Niu P, Zhan F, Ma X, Wang D, Xu W, Wu G, Gao GF, Tan W; China Novel Coronavirus Investigating and Research Team. A Novel Coronavirus from Patients with Pneumonia in China, 2019. N Engl J Med. 2020 Feb 20;382(8):727-733. doi: 10.1056/NEJMoa2001017. Epub 2020 Jan 24. PMID: 31978945; PMCID: PMC7092803

Zheng D, Liwinski T, Elinav E. Inflammasome activation and regulation: toward a better understanding of complex mechanisms. Cell Discov. 2020 Jun 9;6:36. doi: 10.1038/s41421-020-0167-x. PMID: 32550001; PMCID: PMC7280307.